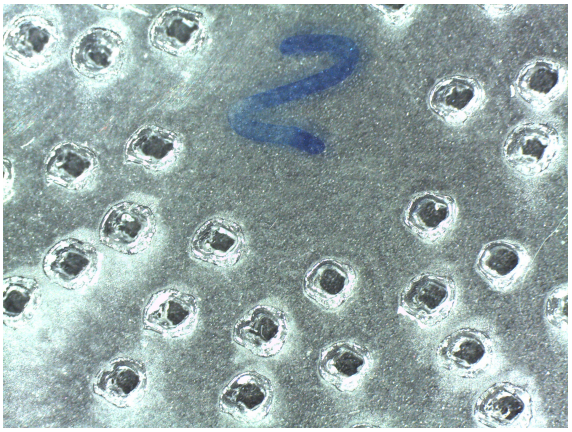

(a) Case 2 methacrylate panel

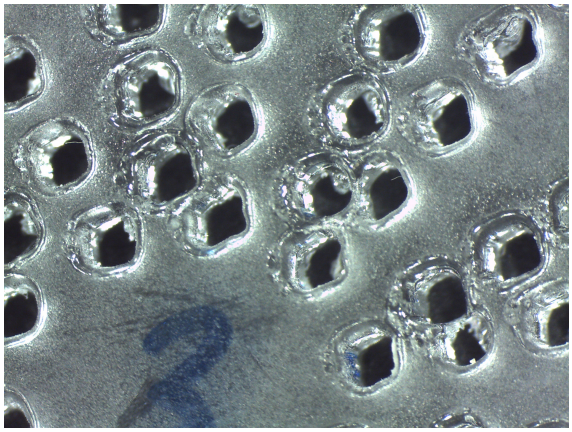

(b) Case 3 methacrylate panel

Figure 5.1: Irregular perforations in the panels for cases 2 and 3.

(Figure 5.2a). While most of these bumps can be manually removed using tools like a needle, punch, or small-diameter drill bits, attempts to remove some of them in panels with a higher thickness resulted in cracks forming in the panels, of around 2-2.5 mm in length (Figure 5.2b).

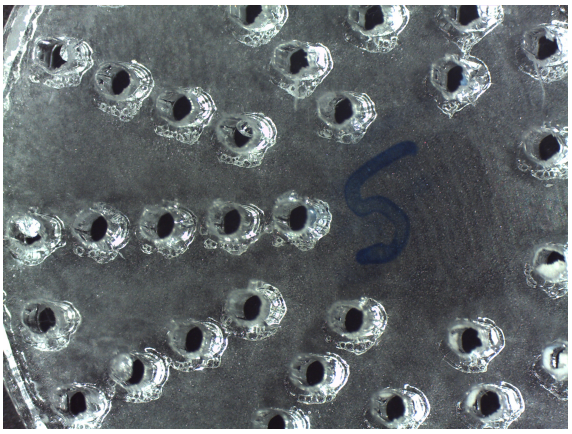

(a) Bumps of material in the Case 5 methacrylate panel

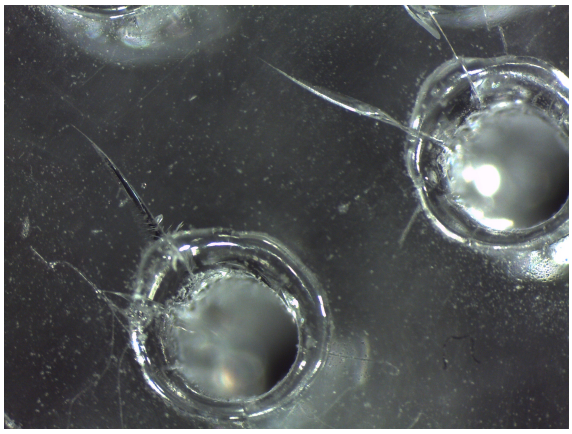

(b) Cracks in one of the methacrylate panel

Figure 5.2: Material bumps and cracks on panels.

In regard to the holes in the 3D printed panels, the main reason that cases 1 to 3 were not printed was due to the small hole diameter of the parameters. A test had been performed previously to check what diameters could the printer do. For this test, a small plate was designed with different diameter holes (Figure 5.3), which range from 0.8 mm to 1.5 mm in increments of 0.05 mm. Using a microscope from Leica microsystems and its software *LAS EZ*, the estimated resulting hole diameter is shown in Table 5.1. The results are an estimation and have a probable error of around 0.05 mm, but in most cases, the resulting diameter in the studied range tends to be between 0.2-0.3 mm smaller than the nominal diameter. Looking at the trends, it can be assumed that the deviation between the nominal diameter and the

resulting diameter decreases as the nominal diameter increases.

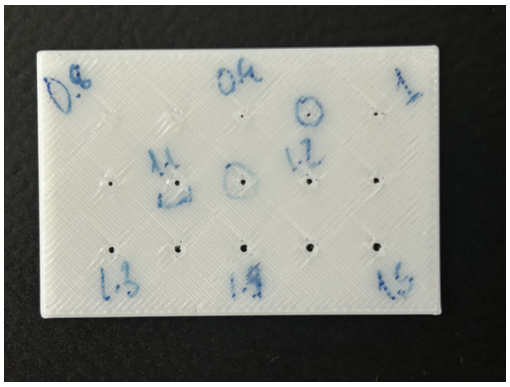

Figure 5.3: Hole diameter test plate.

Table 5.1: Hole diameter test

Nominal diameter (mm)	**Resulting estimated diameter (mm)**
0.9	0.4
1	0.6
1.05	0.7
1.1	0.8
1.15	0.85
1.2	0.9
1.4	1.1
1.5	1.3

As 3D printing is not exact on some aspects of the geometry due to layer deposition and filament height, the diameter of the holes and the thickness of the samples were checked. The diameter of the sample was measured and was 34 mm, as in the CAD model. In Table 5.2, the real values for the thickness of the sample and the estimated diameter of the holes are shown, as well as the nominal values, for comparison. The analytical curves of the results were calculated using the resulting thickness, but the nominal diameter was kept.

Upon examining the tested panels, the perforations appear more circular than those in the methacrylate panels, at least on the top layer. However, on the bottom (or first) layer, the holes exhibit a more complex geometry. As shown in Figure 5.5, some filament portions partially obstruct the perforations, which would likely impact the panel's performance. In Figure 5.4b, the filament completely closes one of the perforations on the first layer, likely due to the heat and expansion of the filament during the printing process. It is important to note that ULTEM™ requires high nozzle temperatures (350 - 380°C) and a heated chamber (120 - 160°C) for successful printing.

While the top and bottom layers of the panel are easily observable, assessing the geometry of the perforations inside the panel is more difficult. The nature of FDM manufacturing

Table 5.2: Resulting thickness and estimated diameters in the tested panels

	Nominal diameter (mm)	Nominal thickness (mm)	Resulting estimated diameter (mm)	Resulting thickness (mm)
Case 4	0.8	3	0.5	3.34
Case 5	1.0	5	0.6	5.4
Case 6	1.2	8	1.0	8.4
Case 7	1.2	2	1.0	2.26
Case 8	1.2	3	0.95	3.34
Case 9	1.0	2	0.7	2.24
Case 10	1.0	3	0.7	3.4
Case 11	0.9	4	0.65	4.3
Case 12	1.1	6	0.85	6.28

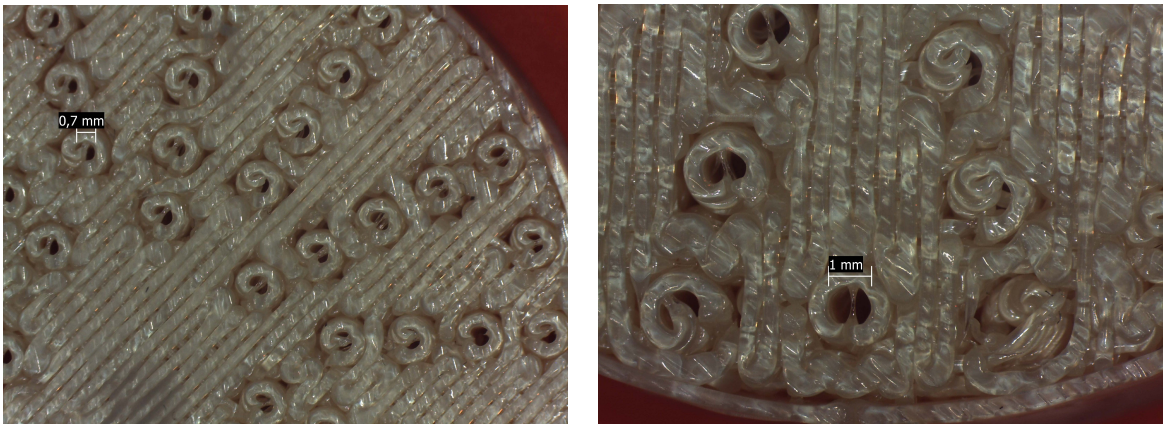

(a) Case 5 ULTEM™ panel first layer (b) Case 6 ULTEM™ panel first layer

Figure 5.4: Irregular perforations in the panels for cases 2 and 3.

would cause the sample to break down if it were attempted to be cut, as the filaments would separate from each other. The same reason as well as the strength of the material makes it very hard to try to remove the parts of the filament that obstruct the perforations. It is reasonable to assume that the perforations are not perfect circular tubes, especially when considering the fine strands of filament that cross through the holes in the top layers. The irregular geometry and incomplete perforations negatively impact the performance of the samples, making it difficult to predict their behavior. This is because both the hole diameter and the perforation area become variables that are difficult to determine accurately.

The gaps and the nature of the layer deposition give rise to porosity in the printed panels, as shown in Figure 5.5. These gaps are particularly prevalent in regions where the perforations are densely concentrated, such as the center of the sample. 3D printers, particularly industrial models like the one used here, are limited in their ability to achieve fine details. Although these printers are highly accurate, they are designed for larger components and are not precise enough to extrude filament into such small spaces, resulting in noticeable gaps. The largest gap identified in all samples measures 0.8x0.8 mm, as seen in Figure 5.5a.

Additionally, the printer's layer height cannot be reduced below 0.254 mm, limiting the ability to refine the sample finish. This constraint leads to imperfections and gaps in the final product. Another contributing factor may be the printing speed. As noted in section 3.2, the printer's speed is fixed at factory settings and cannot be adjusted. If the print is too fast, the filament

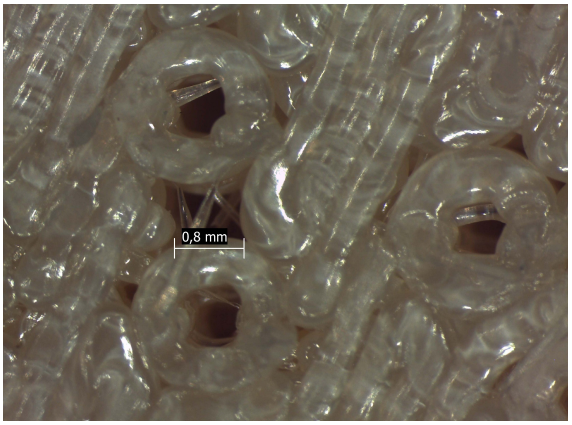

(a) Big gap between two closely situated perforations

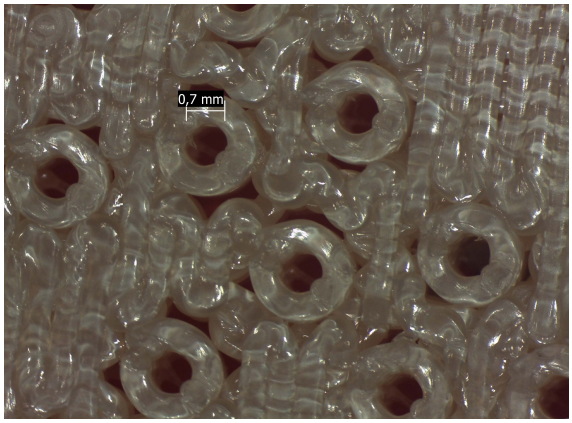

(b) Gaps around most holes

Figure 5.5: Porosity in the tested samples

may not have enough time to properly adhere, leading to under-extrusion and inconsistent deposition. In contrast, printing too slowly can result in stringing and irregular geometries. These factors, combined with the inherent limitations of the printer, contribute to the overall porosity and imperfections observed in the printed samples.

The change in diameter has a direct impact on the perforation ratio. As the diameter decreases while keeping the number of holes constant, the perforation ratio inevitably decreases due to the significant reduction in the size of each individual hole. This results in a lower overall area of perforation relative to the panel. The corresponding perforation ratios for each scenario are presented in Table 5.3. For instance, in the case of the panel in case 4, which initially has 45 holes, the decrease in hole diameter leads to a significant reduction in the perforation ratio. To maintain the original perforation ratio, the number of holes would need to increase to 116, compensating for the decrease in diameter and ensuring that the total perforated area remains consistent with the original design.

Table 5.3: Change in the perforation ratio due to the estimated diameter

Case	**Nº of holes**	**Original Perforation Ratio (%)**	**New Perforation Ratio (%)**
Case 4	45	2.5	0.97
Case 5	70	6	2.18
Case 6	56	7	4.84
Case 7	48	6	4.15
Case 8	48	6	3.75
Case 9	70	6	2.97
Case 10	70	6	2.97
Case 11	57	4	2.08
Case 12	48	5	3.00

The adjusted curves for these panels are presented in Figures 5.6 through 5.14. The modifications in the parameters result in the theoretical absorption peak shifting to a lower frequency. However, the panels in cases 6 (Figure 5.8) and 7 (Figure 5.9) exhibit performance that surpasses expectations, with a higher peak absorption and a broader bandwidth compared to the analytical solution. Additionally, in cases 6, 7, 8 (Figure 5.10), and 12 (Figure 5.14), the theoretical absorption peaks closely align with the experimental peaks. These theoretical values, however, are not entirely realistic because the porosity of the panel has not yet been accounted for. Including porosity would likely increase the absorption values and shift the absorption peak to a higher frequency, making the theoretical results more accurate.

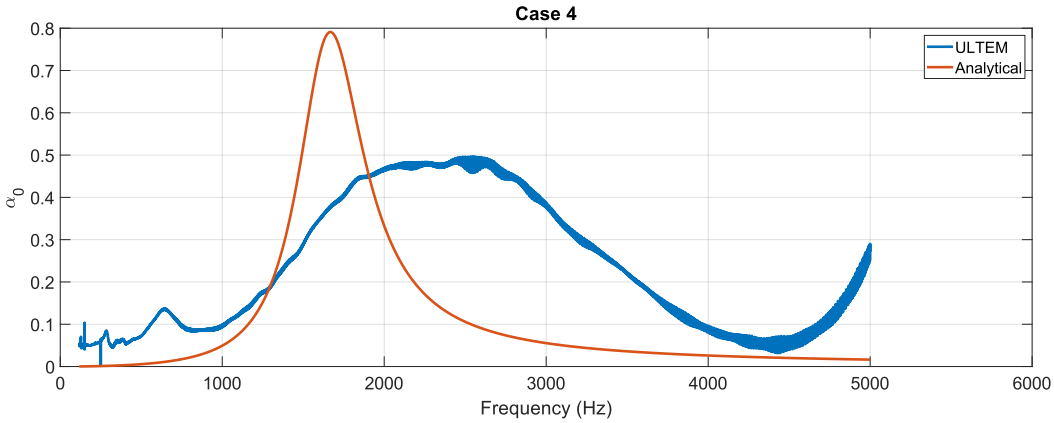

Figure 5.6: Readjusted analytical curve for case 4 for the diameter and percentage ratio.

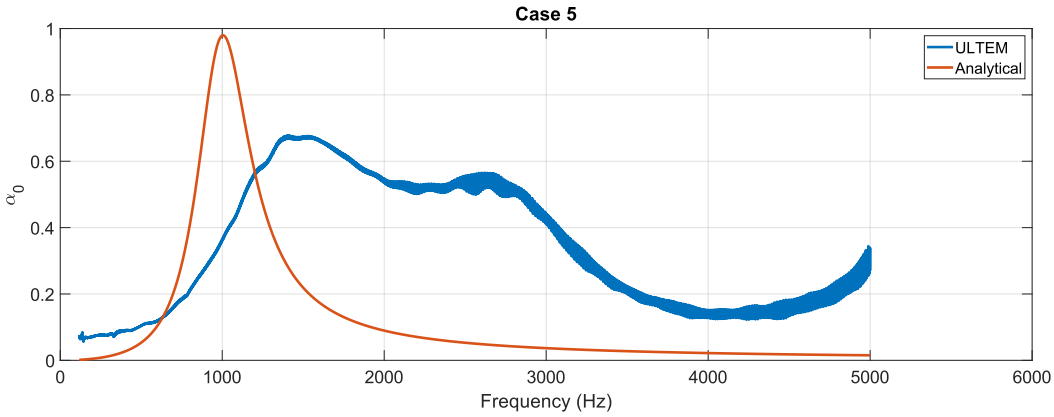

Figure 5.7: Readjusted analytical curve for case 5 for the diameter and percentage ratio.

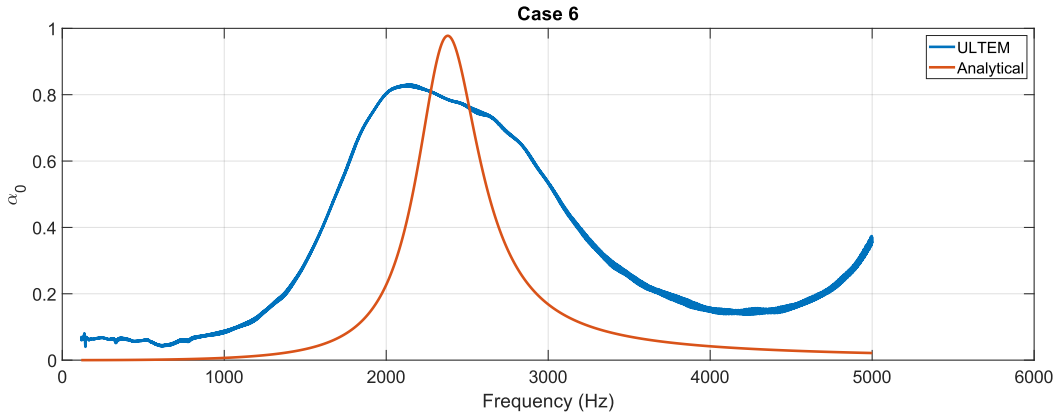

Figure 5.8: Readjusted analytical curve for case 6 for the diameter and percentage ratio.

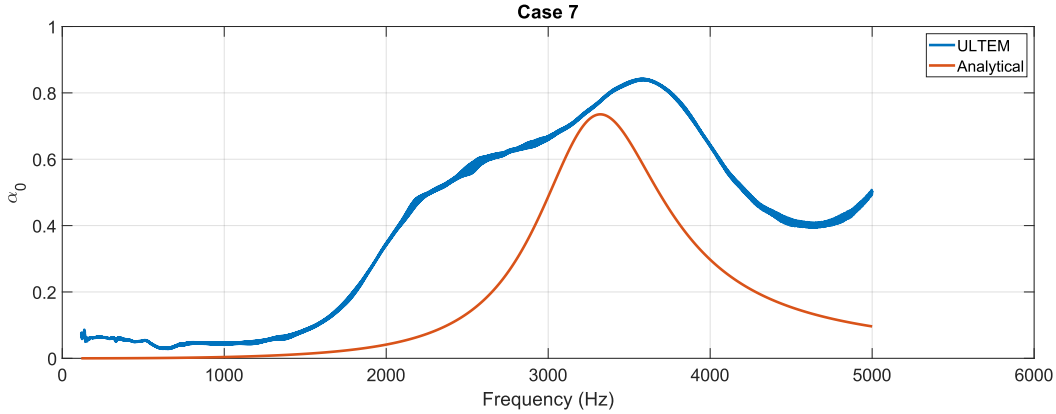

Figure 5.9: Readjusted analytical curve for case 7 for the diameter and percentage ratio.

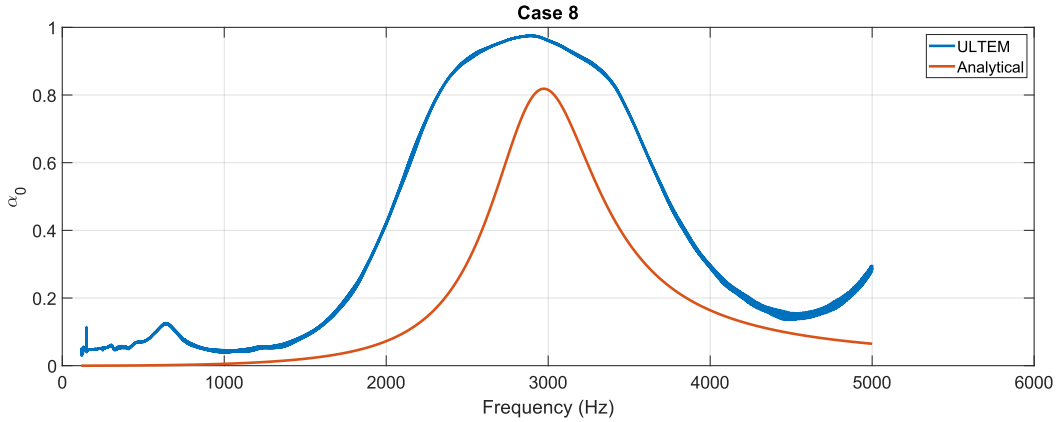

Figure 5.10: Readjusted analytical curve for case 8 for the diameter and percentage ratio.

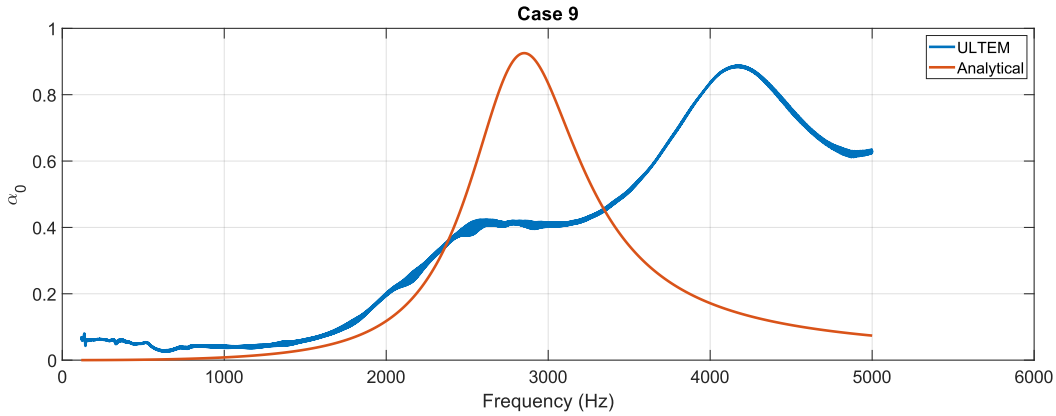

Figure 5.11: Readjusted analytical curve for case 9 for the diameter and percentage ratio.

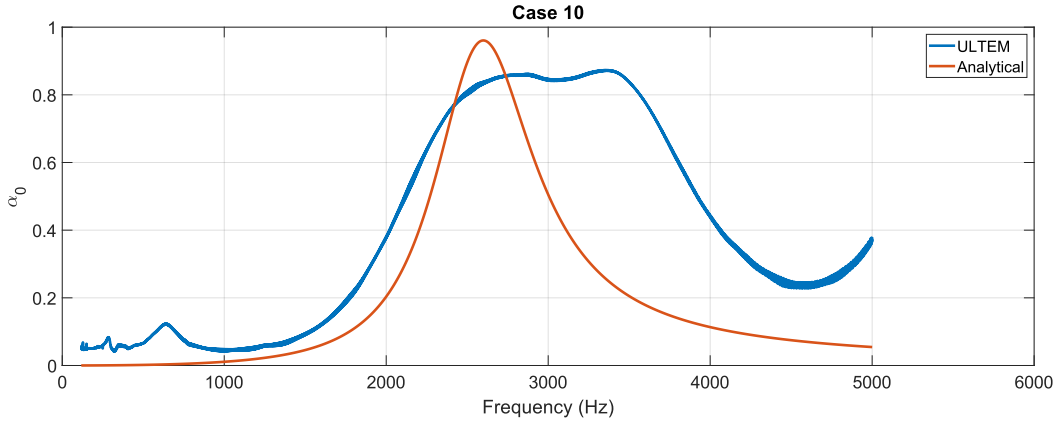

Figure 5.12: Readjusted analytical curve for case 10 for the diameter and percentage ratio.

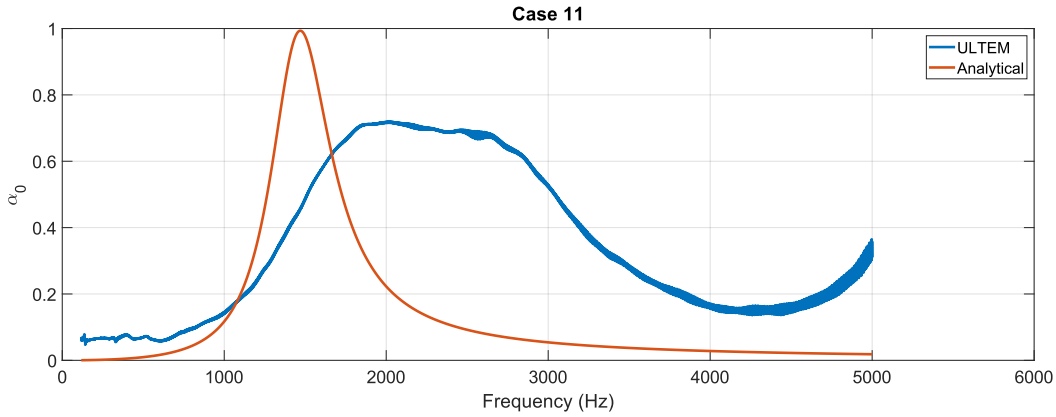

Figure 5.13: Readjusted analytical curve for case 11 for the diameter and percentage ratio.

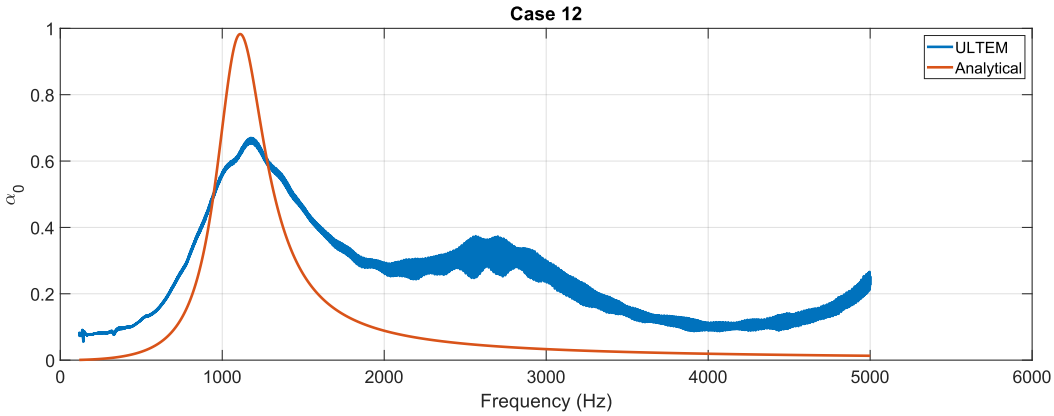

Figure 5.14: Readjusted analytical curve for case 12 for the diameter and percentage ratio.

Porosity of the samples

To accurately interpret the results from the impedance tube test, it is crucial to assess the porosity and the presence of any gaps within the samples. This process involves weighing the samples and comparing their measured mass to the theoretical mass, which is calculated using the density provided in the datasheet. However, calculating the theoretical weight is a complex task because of the variations in the diameter of the perforations throughout the material. While an estimated diameter could be used for these calculations, it would not account for important factors such as the filaments' strings inside the perforations, which may alter the effective cross-sectional area. Additionally, the first layer of the sample could feature obstructions where the filament closes or partially blocks the holes, further complicating the calculation. While these factors must be considered to obtain an accurate evaluation of the sample's structure and its corresponding theoretical mass, it is nearly impossible to include them in the calculations, so a small error must be applied.

One reliable method for determining the density of a sample is by comparing its real volume to the theoretical volume. This can be done using the principle of water displacement. In this process, a graduated cylinder is partially filled with water, and the sample is carefully submerged. It is important to slowly lower the sample into the water and ensure that no air is trapped inside, as this could lead to the formation of bubbles around the object, which would distort the results. When submerged, the sample displaces a volume of water equal to its own volume, causing the water level to rise. By measuring the difference in water levels before and after the sample is submerged, the volume of the sample can be determined.

Once the real volume is measured, it can be compared to the theoretical volume to calculate the density of the sample. Although this method is effective, it becomes less precise when dealing with small samples, particularly when the sample volume is approximately 1 cm^3 for each millimeter height. For such small volumes, the difference between real and theoretical measurements, which could range from 0.1 to 0.9 cm^3, is challenging to detect accurately simply by observing the graduated cylinder.

This issue was demonstrated with one of the samples, as shown in Figure 5.16, where the displaced volume was approximately 2 cm^3. This value is close to the theoretical volume,

which, using the estimated diameter and the measured height, is around 1.97 cm^3. However, with such small components, even slight inaccuracies in decimal places can result in significant errors in the calculations.

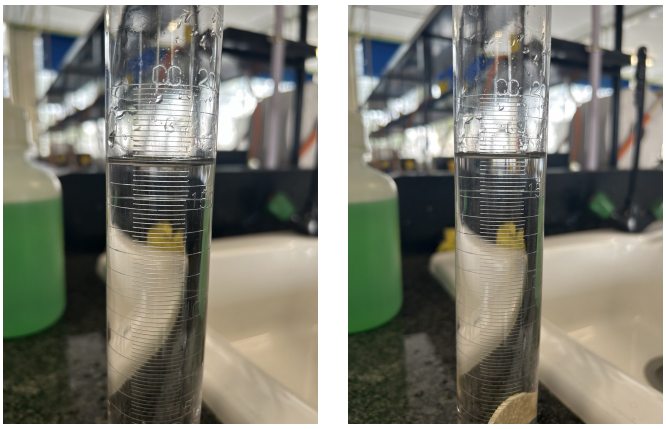

(a) Volume in the cylinder without the sample

(b) Volume in the cylinder with the submerged panel

Figure 5.15: Volume measurement test

Another method for calculating the density of the samples is based on Archimedes' principle, which establishes a relationship between the weight of the sample in air (W_a) and its submerged weight in a liquid (W_f), as shown in Equation 5.1. This principle is grounded in the fact that the buoyant force exerted on a submerged object is equal to the weight of the liquid displaced by the object. The equation also takes into account the densities of both the liquid (ρ_w) and air (ρ_a) under standard conditions, which are essential for accurate calculations. The submerged weight difference between the sample in air and the liquid allows for the determination of its volume and ultimately its density.

$$\rho = \frac{W_a \cdot (\rho_w - \rho_a)}{\rho_w \cdot (W_a - W_f)} + \rho_a \tag{5.1}$$

To carry out this density measurement, a scale equipped with a density kit is used (Figure 5.16a). The procedure begins with placing the sample on the scale to measure its dry weight, W_a. Once the dry weight is recorded, the sample is slowly and carefully submerged into the liquid. It is essential to lower the sample into the liquid gently, ensuring that it is fully immersed without creating air bubbles, which could interfere with the measurement. The sample is then placed into the basket submerged in the liquid, as shown in Figure 5.16b.

The key challenge in this process is to prevent any air from being trapped inside the sample during submersion. If air is trapped within the sample, it would cause a buoyant force that reduces the measured submerged weight (W_f), resulting in an inaccurate density calculation. Therefore, great care is taken during the submersion process to ensure that the sample is fully immersed and free from air pockets. This method provides an alternative and reliable means of calculating the sample's density, which can be cross-verified with other techniques.

(a) Kit set up

(b) Panel submerged in the cylinder

Figure 5.16: Measuring the sample density

To assist in the calculation of the panels' porosity, three circular samples, each with a diameter of 34 mm, were printed. These samples do not have any perforations and each has a different thickness: 2, 3, and 8 mm. Since these samples lack perforations, they are free from the gaps or obstructions that could be caused by the presence of holes, making it easier to compare their real characteristics with theoretical values.Figure 5.17 shows the samples printed for the measurements.

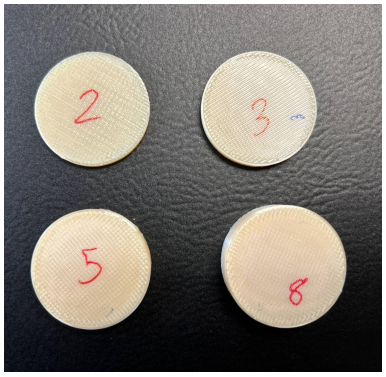

Figure 5.17: Density measurement samples.

By comparing the real weight of these non-perforated samples (which are defined with a 100% fill) with their theoretical weight, as well as with their calculated volume, it is possible to estimate their porosity. This comparison helps to determine the difference between the actual mass of the sample and its theoretical mass if it were fully dense. Once porosity is estimated for these reference samples, the same calculation method can be applied to the perforated samples, allowing for an accurate translation of porosity values to the tested panels.

The results obtained with these samples are illustrated in Table 5.4. The three samples

obtained nearly identical results, 1.22 g/cm^3, with a median deviation of 0.003 g/cm^3. The density stated in the datasheet is 1.27 g/cm^3, which signifies a 3.45% difference. This percentage indicates the intrinsic porosity of the samples.

Table 5.4: Results of the density samples

Nominal height (mm)	**Dry weight (g)**	**Submerged weight (g)**	**Density (g/cm^3)**
2	2,235	0,413	1,226
3	3,364	0,615	1,223
8	8,915	1,666	1,229

The same process was applied to the tested panels, with the results presented in Table 5.5. The median density measured was 1.117 g/cm^3, with a standard deviation of 0.028 g/cm^3. Notably, case 4 stands out, as its density closely aligns with the theoretical and calculated values based on the samples. When isolating its results, the standard deviation decreases to 0.018 g/cm^3 and the median density to 1.11 g/cm^3. Upon examining the sample itself, it is clear that it has a superior finish compared to the others, with no missing filaments in the bottom layer and the holes, if smaller than the nominal value, seem to have no obstructions in them.

Table 5.5: Density of the tested samples

	Dry weight (g)	**Submerged weight (g)**	**Density (g/cm^3))**	**Difference with datasheet (%)**	**Difference with tested samples (%)**
Case 4	3,239	0,490	1,178	7,23	3,93
Case 5	4,987	0,420	1,092	14,03	10,98
Case 6	7,904	0,630	1,086	14,45	11,41
Case 7	2,031	0,222	1,123	11,60	8,46
Case 8	3,071	0,350	1,128	11,16	8,00
Case 9	1,992	0,170	1,093	13,91	10,85
Case 10	3,005	0,285	1,105	13,02	9,93
Case 11	4,136	0,454	1,123	11,57	8,43
Case 12	6,154	0,711	1,131	10,98	7,82

The density obtained can be compared to the datasheet and to the median result of Table 5.4. While comparing the results with the datasheet gives the overall porosity of each sample, comparing it to the latter shows an approximation of the gaps and irregularities created during the manufacturing process.

As with the different perforation, the analytical calculations have to be readjusted to account for the porosity. The perforation rate is exchanged with the percentage difference in density with the test samples. As the equivalent fluid model is used, the irregularity in the perforations could be expected to modify the flow resistivity and geometrical tortuosity. In their research, Cobo and Montero de Espinosa [102] considered the modified resistivity and tortuosity:

$$\sigma_{mod} = \alpha_\sigma \cdot \frac{8\eta}{\phi r^2} \tag{5.2}$$

$$\alpha_{\infty,mod} = a_{\alpha_\infty}\left[1 + \frac{0.85d}{t}(1 - 1.14\sqrt{\phi})\right] \tag{5.3}$$

where α_σ and a_{α_∞} are numbers close to 1. These modifications are included in the code for the analytical curve. The value for the correction parameters is $[\alpha_\sigma, a_{\alpha_\infty}] = [0.5, 1.8]$. The results for the second adjustment are shown from Figures 5.18 to 5.26. While the correction parameters should be different for each case, the intention was to find one set of values that could adjust the closest to most analytical curves to their respective experimental curves, to find a pattern in the ULTEM ™. These values suggest that the flow resistivity decreased by 50% and the geometrical tortuosity increased by 80%. According to Mechel [241], the resistivity is inversely proportional to the face velocity of the flow through the panel, so the increase in value can be interpreted as an increase in velocity. The tortuosity is a function of the correction length induced by the radiation of the air column inside the pores in the air [75], so the effect of this parameter can be interpreted as a lengthening of the correction length.

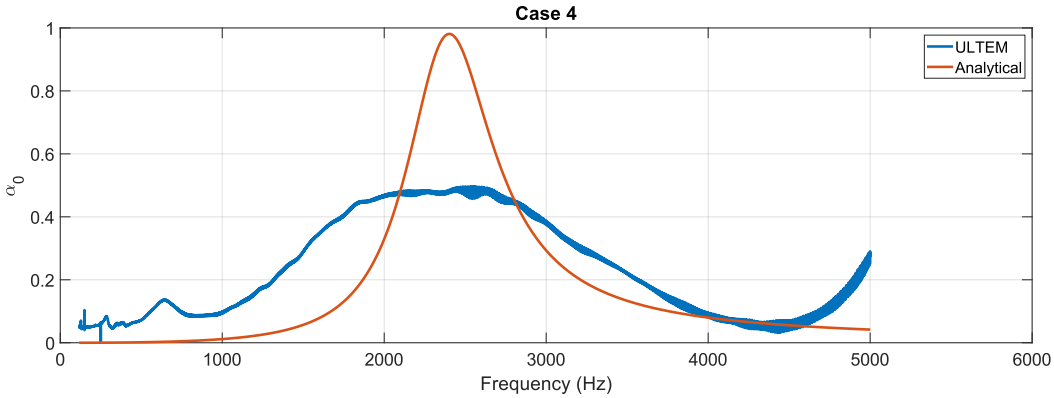

Figure 5.18: Readjusted Case 4 panels with the porosity and correction parameters.

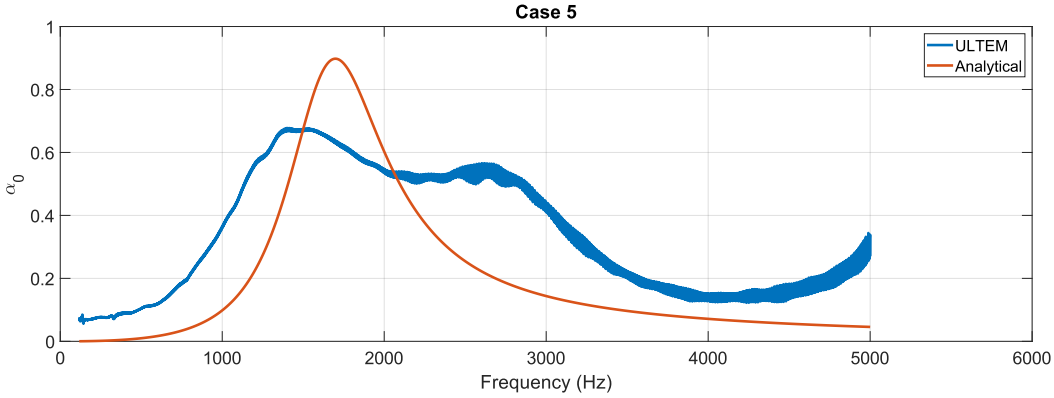

Figure 5.19: Readjusted Case 5 panels with the porosity and correction parameters.

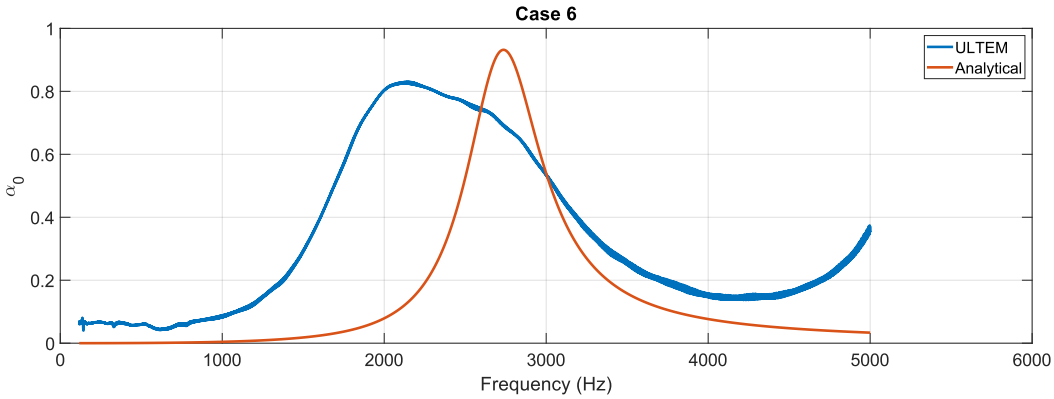

Figure 5.20: Readjusted Case 6 panels with the porosity and correction parameters.

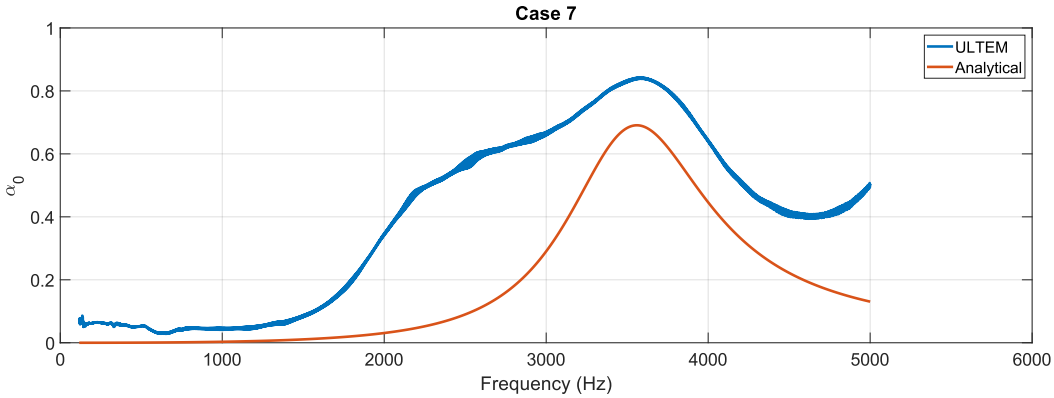

Figure 5.21: Readjusted Case 7 panels with the porosity and correction parameters.

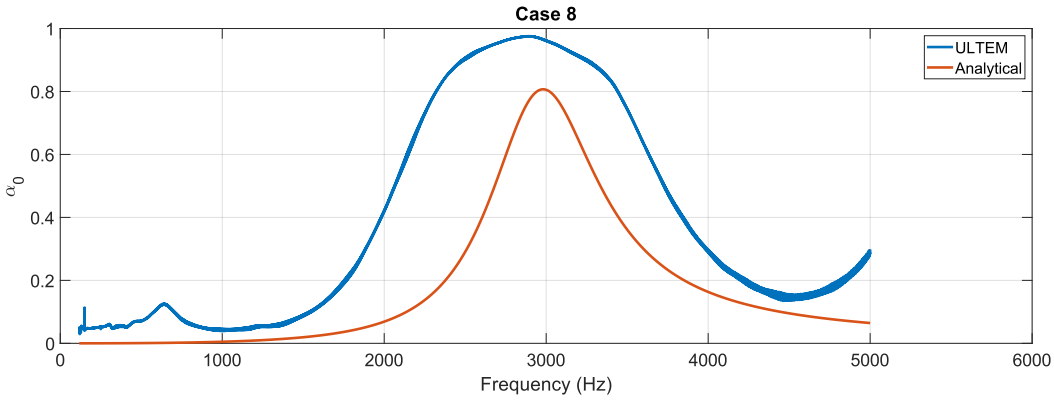

Figure 5.22: Readjusted Case 8 panels with the porosity and correction parameters.

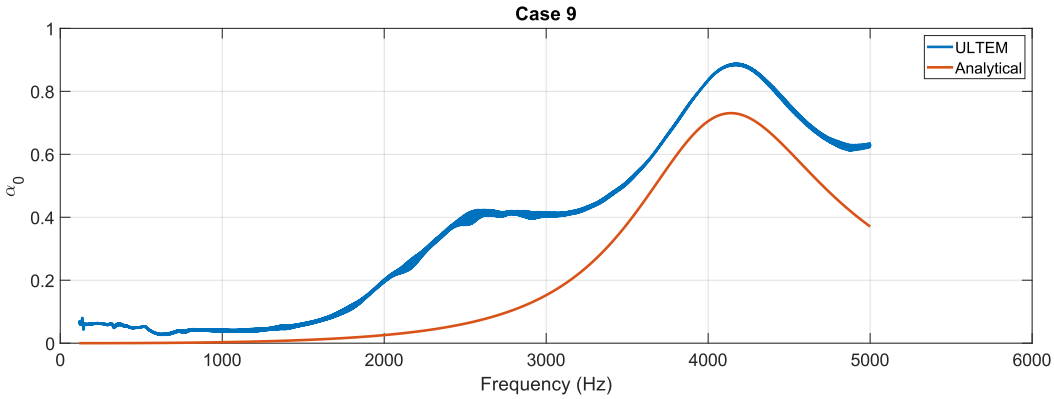

Figure 5.23: Readjusted Case 9 panels with the porosity and correction parameters.

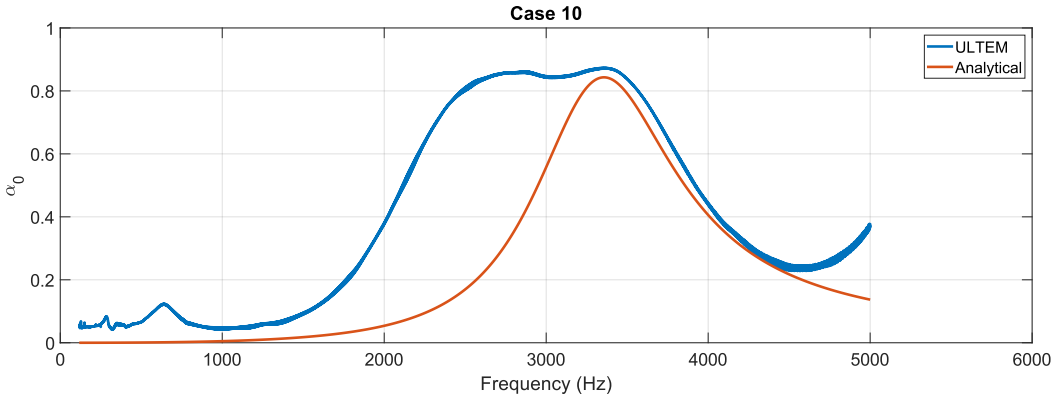

Figure 5.24: Readjusted Case 10 panels with the porosity and correction parameters.

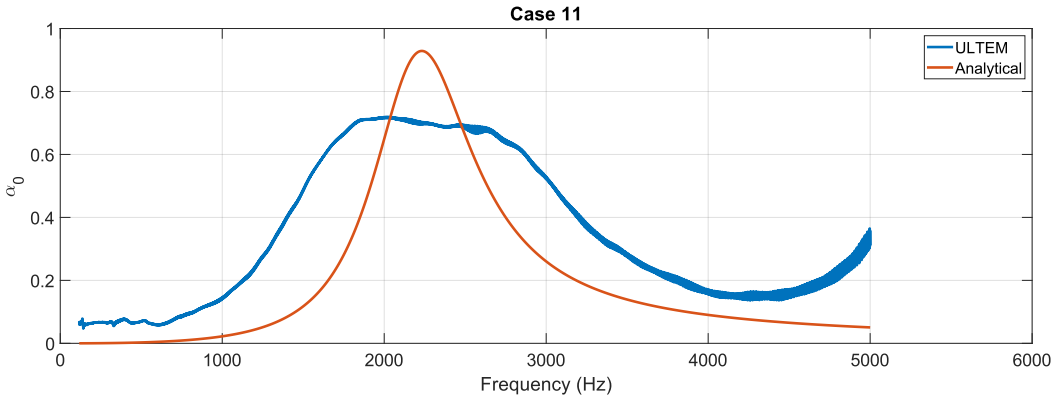

Figure 5.25: Readjusted Case 11 panels with the porosity and correction parameters.

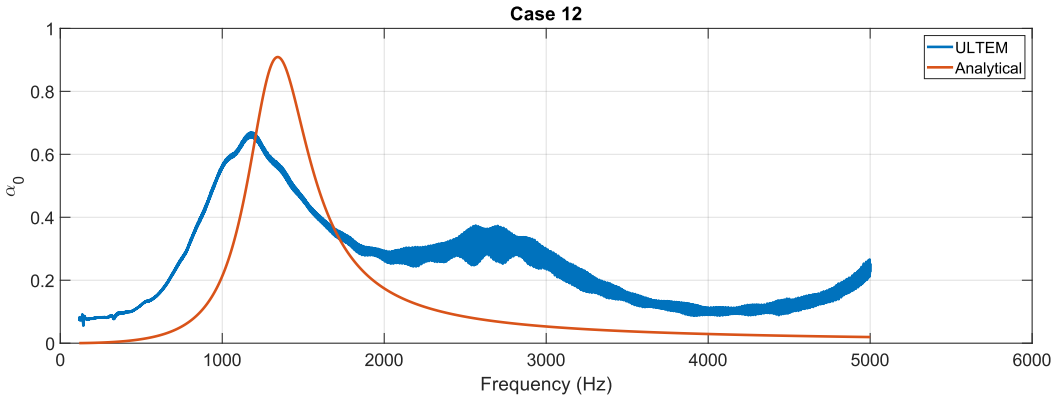

Figure 5.26: Readjusted Case 12 panels with the porosity and correction parameters.

Adjusting the percentage ratio value to reflect the porosity of the sample and applying correction factors reduces the absorption peaks in Cases 9 and 10, aligning them more closely with the experimental curves. In all cases—except for Cases 5, 6, and 12—the frequency at which the absorption coefficient peaks remains nearly identical to the analytical predictions.

For cases where the peak spans a broad range with a relatively constant value (see Figure 5.25) or where two small consecutive peaks appear (see Figure 5.24), the peak is identified as the center of the broad range or the highest of the two peaks, respectively. However, fully replicating the experimental absorption curve remains challenging, if not impossible. Small peaks at low frequencies, as well as valleys that form while the absorption coefficient increases (in Case 9) or decreases (in Case 12), are difficult to predict accurately. Additionally, some tested panels behave like multi-layer configurations, exhibiting multiple peaks. This complexity makes analytical replication challenging due to the influence of the cavity distance parameter.

The width of the peak determines the breadth of the absorption band, which is defined as the region where the absorption coefficient exceeds 0.5. As previously noted, test results show that the samples have significantly wider absorption bands than expected. Notably, Cases 5 and 11 exceed 1 octave. While still relatively low, this is understandable given that the primary objective was to evaluate the feasibility of the manufacturing method rather than optimize the samples. In comparison, an optimized single-layer MPP would typically achieve an absorption bandwidth of around 2 octaves.

Among the remaining samples, most—except for Cases 4 and 12—exhibit absorption bandwidths between 0.8 and 0.9 octaves. Case 4, however, does not provide any meaningful absorption, as its curve never surpasses the 0.5 threshold at any point.

Comparison with other additive manufacturing materials

To analyze the error of the FORTUS 450mc printer, cases 4, 6, 7, and 9 were tested again using two different new materials. These panels were manufactured by the Italian company Weerg, one of the world's largest 3D printing facilities, as UPM did not have the equipment to do so. One of the materials used is PEEK, an aerospace-certified thermoplastic polymer. The second one is ceramic resin, Ultracur3D RG 3280. Some types of ceramics are accepted for

space use, some of which are usually used for 3D printing. The panels made of PEEK were manufactured using FDM, while the ceramic resin panels were manufactured using MSLA (Masked SLA). An MSLA printer works similarly to SLA printers but uses a different method for curing the resin. Instead of a laser, it uses a liquid-crystal display (LCD) to project UV light onto the resin, curing it layer by layer. The LCD has an array of pixels that either block or allow UV light, curing the resin in the desired pattern to construct the object.

One notable characteristic of resin printers is that they cannot print directly on the bed due to the layer curing process. The print bed starts at the bottom of the resin tank, and each layer of resin is selectively exposed to light to harden into the desired shape. After each layer cures, the bed moves upward, allowing fresh resin to flow beneath it for the next layer. Since the resin is liquid before curing, supports are necessary to hold the structure in place during printing. To minimize the number of supports and prevent marks from appearing on one side—marks that could affect the sample's performance—the panels were printed in a vertical orientation. The resulting marks from the printing process are shown in Figure 5.27, and it is not likely to have any effect on the experimental results.

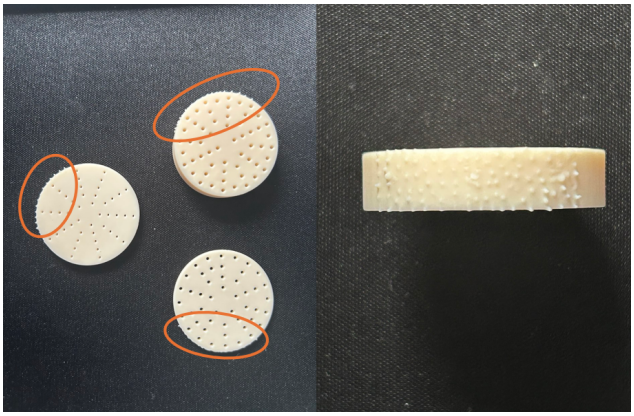

Figure 5.27: Printed supports location for the ceramic resin panels.

Printing the samples in this orientation has one result: due to the perforation diameters being too small to accommodate supports, the perforations in the final product appear oval-shaped, as shown in Figure 5.28a and Figure 5.28b, which also show the region where the print supports were placed.

The measured diameters are presented in Table 5.6. The variation in diameters for cases 6 and 9 of the PEEK samples can be attributed to the panel containing holes of different diameters, as illustrated in Figure 5.29. Specifically, the range observed in the PEEK samples reflects the presence of multiple hole sizes within the same panel. In the case of the ceramic resin panels, the range in diameters corresponds to the two average diameters of the ovals that were measured in the holes, highlighting the variation in shape and size of the openings. This distinction is important for understanding the variation in measured values and their potential impact on the performance or characteristics being studied.

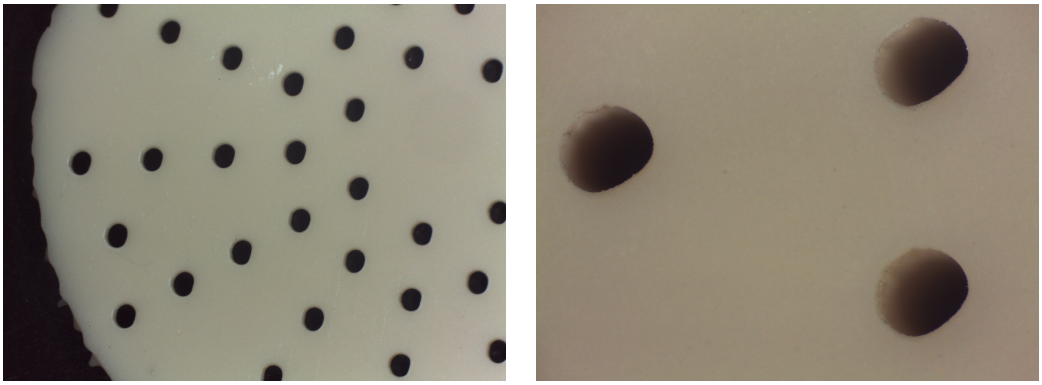

(a) Case 9 panel. (b) Case 6 panel.

Figure 5.28: Ceramic resin panels

Table 5.6: Diameter of the perforations in the PEEK and Ceramic Resin panels.

Case	**PEEK**	**Ceramic Resin**
Case 4	1.1 mm	0.7 mm
Case 6	1.55 mm ±0.5 mm	1.2 mm
Case 7	0.9 mm ±1 mm	1.15 mm ±0.05 mm
Case 9	1 mm ±2 mm	0.95 mm ±0.05 mm

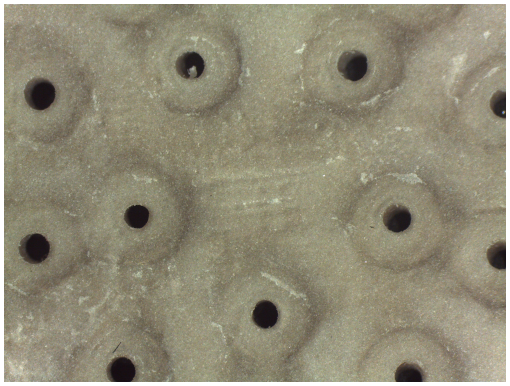

Figure 5.29: Case 7 panel made of PEEK, with different perforation diameters.

There is a noticeable difference between the first and last layers of the PEEK samples compared to the ULTEM™ samples, as shown in Figure 5.30. In the PEEK samples, there is no visible gap around the perforations caused by filament deposition, unlike in the ULTEM™ samples, and there is no obstruction in the perforations. There are small areas missing material in the first/bottom layer of the sample, especially around some of the perforations in the case 6 panel (Figure 5.31a). There are also types of marks that could lead one to believe that there were some post-processing operations done on the panels to achieve a better end product. These marks can be seen around the perforations, and, in one case, there is material extruding up from the borders of one perforation. After contacting the company that made the PEEK

and ceramic resin panel, Weerg, it was confirmed that the PEEK panels came out with obstructions (the holes were partially closed) and, therefore, had to be reworked.

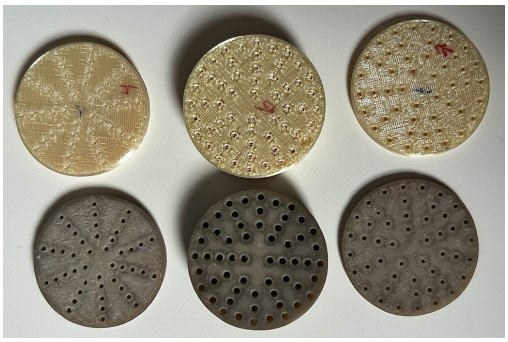

Figure 5.30: Comparison in finish between the ULTEM™ (top) and PEEK (bottom) panels.

In Figure 5.31b, a small piece of material is visible inside one of the holes, but it can be easily removed. The perforations themselves are also more consistent in shape (circular), with the only issue being the variation in diameters within a single panel, as mentioned earlier, and clearly seen in the case 7 panel. Unlike the FORTUS 450mc printer, where the resulting diameter tends to be smaller, in cases 4 and 6, the diameter is actually larger. For cases 7 and 9, the diameter is closer to the nominal value. Slightly smaller in case 7, decreasing from 1.2 mm to 0.9 mm on average. In case 9, the nominal diameter is 1 mm, which is the average diameter in the PEEK panel.

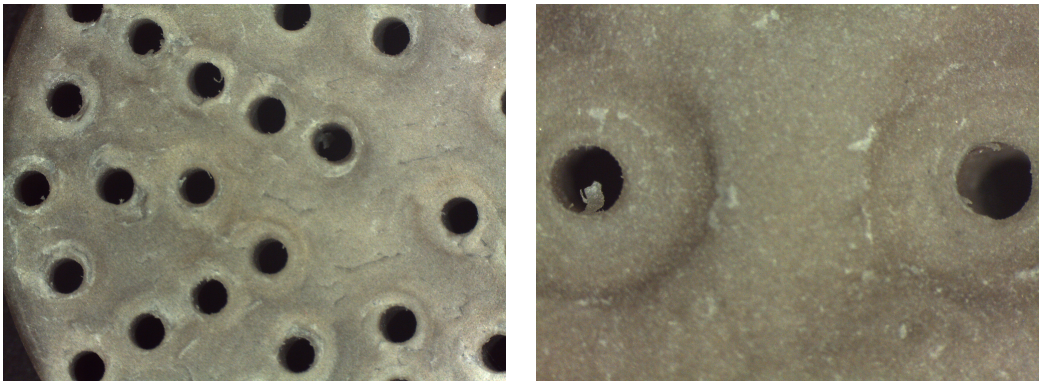

(a) Missing material. (b) Material inside the perforation.

Figure 5.31: PEEK panels

The comparison between the three materials in the four panels can be seen from Figure 5.32 to Figure 5.35. The analytical solution, which uses the nominal original values without applying any correction parameters, is also included in the figures. This inclusion serves as a baseline reference, enabling a direct comparison between the results from the manufacturing methods and the theoretical predictions. The primary objective of this comparison is to assess the accuracy of the manufacturing processes, identify any discrepancies, and evaluate how closely the actual performance of the materials aligns with the expected outcomes based on the analytical solution. By analyzing these figures, one can gain insight into the reliability

and precision of the manufacturing techniques for each material, facilitating improvements or adjustments where necessary.

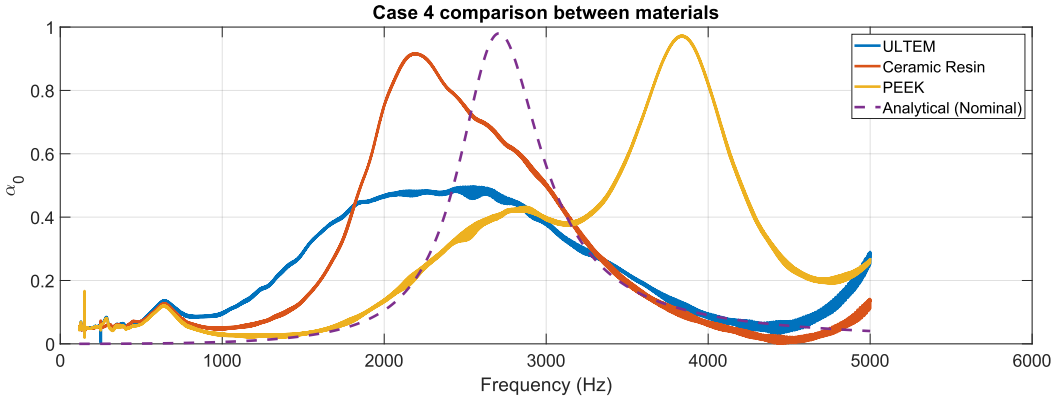

Figure 5.32: Case 4 panels with three different AM materials.

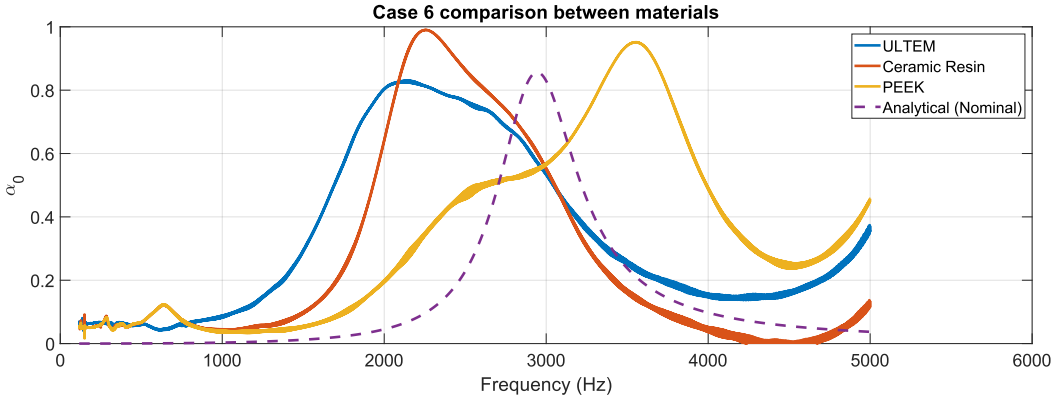

Figure 5.33: Case 6 panels with three different AM materials.

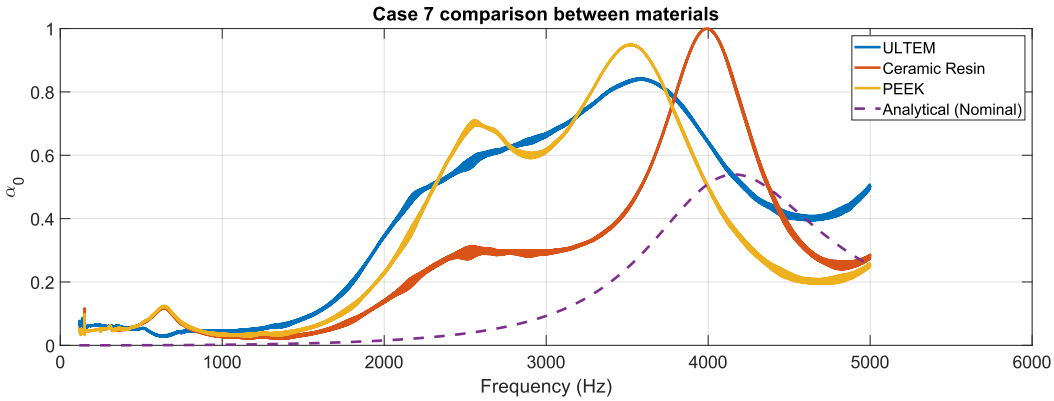

Figure 5.34: Case 7 panels with three different AM materials.

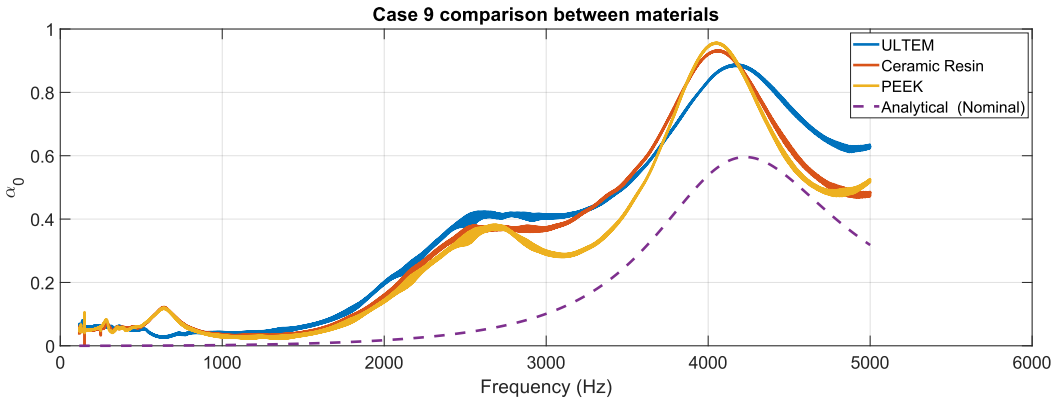

Figure 5.35: Case 9 panels with three different AM materials.

The tests show a variety of different curves between the three materials. Only in the Case 9 panels (Figure 5.35) can we observe similar curves, with the ceramic resin and PEEK panels having near-identical absorption peaks and a very similar curve. The ULTEM™ curve is also very similar in peak and curve, the main difference being a slightly lower peak and its displacement to the right. Despite the similarity in the curves, the hole diameters vary across materials: PEEK has a perforation diameter of 1 mm, ceramic resin has 0.95 mm, and ULTEM™ has 0.7 mm. The thickness of the PEEK and ceramic resin panels is 2 mm, while ULTEM™ panels are slightly thicker at 2.24 mm. Though there are no visible gaps or pores, it is important to note that this does not rule out the presence of porosity. 3D printed materials are inherently porous, and in ceramic resin components, pore sizes can range from micrometers to millimeters. The samples obtain a higher absorption coefficient than the analytical solution predicted. The absorption peak is around a similar frequency: 4060 Hz for the PEEK and the ceramic resin panels, 4190 Hz for the ULTEM™ and 4230 Hz for the analytical curve.

The next instance where the results show some degree of similarity is in Case 7 (Figure 5.34), though the comparison is limited. The only commonality is the location of the absorption peak. The ULTEM™ and PEEK samples display closely matching results, but the ceramic resin peak is shifted by nearly 500 Hz, occurring later than the peaks of the other two materials. In this case, the analytical curve's peak lies beyond the peaks of the samples, at 4180 Hz, closer to the ceramic resin panel, which is 4000 Hz.

In Cases 4 and 6, the ceramic resin and ULTEM™ samples share similar peak locations. However, the PEEK sample in these cases shows distinctly different results. In Case 6, while the ceramic resin and ULTEM™ curves align quite well, the ceramic resin panel's absorption peak is found 200 Hz later than the peak of the ULTEM™ panel. The difference in results can be easily explained by the significant difference in diameters in those two cases.

The goal of microperforated panels (MPPs) is to achieve the highest possible absorption coefficient at a specific frequency, typically aligning with the natural frequency of the component they are designed to protect. These panels demonstrate strong absorption peaks exceeding 0.8—except for the ULTEM™ sample in Case 4—which are promising results, occasionally surpassing expectations (as seen in Cases 7 and 9). However, their limited

absorption bandwidth has driven research into multilayer MPPs, which have been shown to expand the bandwidth to over four octaves in triple-layer configurations.

Among the tested samples, the ceramic resin panels exhibit the highest manufacturing accuracy relative to their CAD models, meaning their performance should closely match theoretical predictions. Across the four cases, the analytical curve aligns more closely with these samples, though notable discrepancies remain. In particular, the ceramic resin panels exhibit peak frequency shifts to the left, with the largest deviation occurring in Case 6 (approximately 700 Hz) and the smallest in Cases 7 and 9 (around 150 Hz). While the diameter differences are minor, variations in perforation shape and the intrinsic porosity of ceramic resin may be key factors contributing to these deviations.

Except for the ULTEM™ sample in Case 4 and the PEEK sample in the same case, all other samples exhibit a broader absorption band than expected. Theoretically, Case 4 should have the widest absorption band at 0.33 octaves. However, the tested samples deviate from this prediction, displaying absorption bands at least twice as wide as the analytical model suggests. In the other three cases, the ULTEM™ samples exhibit the broadest absorption bands, ranging from 0.7 to 0.9 octaves. Meanwhile, the ceramic resin samples, which more closely align with the analytical predictions, demonstrate a narrower bandwidth.

Chapter 6

Conclusions and future work

The work presented in this Doctoral Dissertation aimed to test and analyze the utilization of additive manufacturing materials such as ULTEM™ and methods such as Fused Deposition Modeling in the creation of microperforated panels, with the objective of reducing the transmission of acoustic vibrations in the payload fairing of launchers, to protect the payload it would carry. For this, the proposed materials, ULTEM™ 9085 and 1010, manufactured with the FORTUS 450mc printer from STRATASYS, were mechanically characterized first. A good understanding of the mechanical properties provides the knowledge to extract the highest performance possible from the materials. It also allows the possibility of understanding the printer's capabilities. The machine used is an industrial printer, which means the only parameters that are user-controlled are the filament orientation and the percentage of infill, as the only other possible shape of the infill is the hexagram. The thickness of the outer walls can also be controlled, but the only possible layer heights are 0.254 mm and 0.33 mm, which depend on the extruder mounted on the printer.

While an industrial printer does not allow for much freedom, in contrast with the many printers using open source software that are easily available, they have other advantages. STRATASYS provides engineering-grade quality, accurate and reliable performance, but it is mostly aimed at transforming supply chains, accelerating manufacturing, and reducing production costs. The FORTUS 450mc printer offers a large range of materials, including the high-performance thermoplastic ULTEM™, tested in the present work, and has a large build volume, which enables the production of larger parts or multiple iterations. The material characterization tests show good repeatability, with a low standard deviation between the samples of the same type (1A flat, 5A on-edge, etc.), taking into account that 3D materials are anisotropic. The volume of the printer allowed for many of the samples to be printed at the same time, which, even if it reduced the production time, may have been detrimental to the performance of some of the samples. A 3D printer goes layer by layer, so, by the time that the upright samples are printed, the flat and on-edge samples would have spent an extra hour or two at the high temperature that the chamber requires for printing. ULTEM™ 9085 and 1010 are more than capable of sustaining high temperatures before reaching a critical point, but the properties may have been affected.

While the porosity was only calculated for acoustic test samples, the results can also extrapolate

to the mechanical tests. Although the density test was performed on three of the same geometries but different thicknesses, the three obtained almost identical density values, which indicated a 3% porosity when compared to the datasheet value. It is fair to assume that the samples of the mechanical test would have a similar porosity, as the geometry in 3D printed components is an important factor. That's the main reason the acoustic samples had a significantly lower density than the density test samples, as the holes caused the infill not to be the 100% which was defined. The effect that both shape and porosity have on the mechanical properties is the reason for the differences of the tests with the material's datasheet, either increasing the tensile strength or decreasing the samples' elasticity.

When it came to the creation of microperforated panels through the use of additive manufacturing methods such as FDM, these issues became more apparent, especially with an industrial printer. While incredibly precise, it is not meant to do these types of perforations. Although the diameter of the perforations can be controlled and predicted after a few test runs, a good percentage of the holes will have filament on them; there is a limit on how small the diameter can be, and if the desired percentage ratio is high, the printer will have more issues. The printer would be unable to fill the gaps between holes correctly, either leaving the gap completely, increasing the porosity, or enclosing the holes, reducing the perforation ratio.

Without even getting into the results of the acoustic tests, the finalized product that came to be using MSLA in comparison with the FDM samples is superior. The ULTEM™ and the PEEK samples had issues with the holes. The issues with ULTEM™ have been documented in this dissertation, but the issues with PEEK, similar to ours, were dealt with by the company that made them by reworking them. Drilling in plastic usually causes more problems, as it creates heat and could deform the component. On the other hand, the resin samples do not show any issues replicating the geometry in the CAD model. The nature of the manufacturing process and the small diameter of the perforation cause the shape of the perforation to be more oval-shaped instead of circular. The preciseness of MSLA makes the performance of the panels easier to predict, as the shape of the perforations can be adjusted in the equations and the porosity of the ceramic resin can be calculated as well. Now, while ULTEM™ and PEEK are certified for space applications, the question remains about ceramic resins.

The European Cooperation for Space Standardization (ECSS), in the document ECSS-P-ST-30, specifies what materials are acceptable for space use. Regarding ceramics, the materials typically accepted are: Silicon Carbide (SiC), Alumina (Al_2O_3), Zirconia (ZrO_2), Silicon Nitride (Si_3N_4), Titanium Diboride (TiB_2), Boron Nitride (BN), and Magnesia (MgO). The first three are typically used in additive manufacturing. The exact composition of Ultracur3D RG 3280 is not known, as it is not publicly shared, the only information available being that its weight has around 65% of silica. What we know of the material is that it is a rigid polyurethane-based resin, which generally exhibits low outgassing compared to other types of resins, but the specific formulation of Ultracur3D RG 3280 would let us know how it would behave. The datasheet provided by the company did specify that it was subjected to outgassing tests, following the NASA ASTM E595-15 standard, which it passed with a total mass loss of less than 0.1%. The mechanical properties are also good, with a 10 GPa Young's modulus, a 76 MPa tensile strength, and a heat deflection temperature of over 280º, which makes it a good alternative to metals in space applications.

Despite the challenges inherent to the FDM process, the panels still achieve good overall performance. They exhibit strong absorption capabilities and broad peaks without the need for extremely small perforation diameters. However, the primary issue with using FDM for MPPs lies in predicting their behavior accurately. The final printed structure often deviates from the original design, and while adjustments can be made to the design parameters, additional factors must be incorporated into the mathematical model for better accuracy.

The application of correction parameters helped bring the analytical curves closer to the experimental results, with many following similar trends. However, the inconsistencies between the curves appear somewhat random. While FDM-produced panels demonstrate promising performance, the inability to predict their behavior reliably introduces uncertainty. With advancements in 3D printing technology, particularly higher-precision printers, FDM could become a viable alternative—especially if the final product more closely matches the intended design.

Currently, the high extrusion temperatures required for certain filaments may contribute to hole obstructions. Improvements in layer height control and print speed regulation could enhance the accuracy of microperforated panel manufacturing. However, at present, resin-based printing and CNC machining appear to be more reliable options. That said, FDM could still serve as a strong alternative to metal components in other types of acoustic vibration reducers, such as Helmholtz resonators. These structures often feature complex geometries but are larger and do not require microperforations, making them better suited to FDM manufacturing.

Future work

There are many parts in this dissertation that can be expanded upon with future work. A further and deeper study of the mechanical properties of ULTEM™ 9085 and 1010 is essential to understand how these materials perform under extreme environmental conditions, particularly those encountered in space applications. This expanded study would involve performing a series of mechanical tests on these materials after they have been subjected to both hot and cold extreme temperatures. These temperature extremes are common in space environments, where materials are exposed to severe temperature fluctuations during missions, including exposure to direct sunlight and the cold vacuum of space. This study would focus on a comprehensive analysis of how these temperature fluctuations influence their structural integrity. Furthermore, the study would include a detailed investigation into the role of porosity and its effect on the mechanical properties of ULTEM™ 9085 and 1010. Porosity in materials can significantly affect their strength, durability, and overall performance, particularly under stress or in environments with extreme temperature variations. Analyzing the size, distribution, and volume of pores in the material would provide insight into how porosity influences mechanical properties such as fatigue resistance, fracture toughness, and overall structural performance. Understanding the interplay between porosity and thermal effects would be crucial for optimizing the use of these materials in applications where material failure could have catastrophic consequences.

Studying the use of ULTEM™ in other types of acoustic vibration reducers, such as Helmholtz

resonators or spring-dampers, presents an interesting opportunity to explore its potential in applications where traditional microperforated panels may not be the ideal solution. Both Helmholtz resonators and spring-dampers are widely used for controlling acoustic vibrations in various industries, and their geometry can be more compatible with Fused Deposition Modeling (FDM) 3D printing techniques, making them prime candidates for experimentation with ULTEM™ materials. With its high strength, thermal stability, and excellent damping properties, ULTEM™ could improve the performance and reliability of these components in environments where traditional materials or manufacturing techniques may fall short.

The use of ceramic resins like Ultracur3D RG 3280 for creating microperforated components has yielded excellent results, owing to their high precision and capability to produce intricate geometries. Using additive manufacturing with these ceramic-based resins (SLA/MSLA) offers a level of accuracy in creating microperforations that surpasses what is achievable with FDM technology. As the demand for high-performance acoustic materials continues to rise, a more in-depth analysis of these specialized resins becomes crucial for advancing the development of microperforated panels, optimizing their acoustic properties, and meeting the evolving needs of various industries.

Referencias

[1] RL Radcliffe. *Surveyor nose fairing mode survey*. Tech. rep. 1964.

[2] JR Butcher. "The separation test in vacuum of the ARIANE 4 payload fairing". In: *NASA, Goddard Space Flight Center, 15th Space Simulation Conference: Support the Highway to Space Through Testing*. 1988.

[3] Dr Dirk Schwingel et al. "Aluminium foam sandwich structures for space applications". In: *57th International Astronautical Congress*. 2007, pp. C2–4.

[4] Soon-Hong Park. "An overview of acoustic and vibration research activities for the structural development of Korean space launchers". In: *The Journal of the Acoustical Society of Korea* 39.4 (2020), pp. 342–350.

[5] Ryan D'Agostino. "Elon Musk: Why I'm Building the Starship out of Stainless Steel". In: *Popularmechanics. com. https://www. popularmechanics. com/space/rockets/a25953663/elonmusk-spacex-bfr-stainless-steel/(accessed Oct. 10, 2022)* (2019).

[6] Mara S. Escartí-Guillem, Lluis Miguel Garcia-Raffi, and Sergio Hoyas. "Review of launcher lift-off noise prediction and mitigation". In: *Results in Engineering* 23 (2024), p. 102679. ISSN: 2590-1230. DOI: https://doi.org/10.1016/j.rineng.2024.102679.

[7] Malcolm J Crocker. "The vibroacoustics environment of spacecraft during launch and flight". In: *Sound and Vibration* 36.6 (2002), pp. 5–5.

[8] Chongwen Jiang et al. "A review of impinging jets during rocket launching". In: *Progress in Aerospace Sciences* 109 (2019), p. 100547.

[9] C Stavrinidis et al. "Advancements in vibroacoustic evaluation of satellite structures". In: *Acta Astronautica* 48.4 (2001), pp. 203–210.

[10] Zbigniew Rarata et al. "Vibro-acoustic response of spacecraft instrument subjected to diffuse sound field: Numerical simulations and experimental verification". In: *Applied Acoustics* 184 (2021), p. 108338.

[11] S Griffin, S Lane, and D Leo. "Innovative vibroacoustic control approaches in space launch vehicles". In: *Proceedings of Inter-noise*. 2000.

[12] Steven A Lane, Steven Griffin, and Robert E Richard. "Fairing noise mitigation using passive vibroacoustic attenuation devices". In: *Journal of spacecraft and rockets* 43.1 (2006), pp. 31–44.

[13] Jamie Kha et al. "An analytical approach for modelling the vibroacoustic behaviour of a heavy fluid-loaded plate near a free surface". In: *Journal of Sound and Vibration* 538 (2022), p. 117206.

[14] Tomasz Krzyzynski et al. *Modelling and Control Design of Vibration Reduction Systems*. Springer, 2019.

[15] BE Sandman and JE Boisvert. "Simplified structural acoustic characterization of external compliant coatings on submerged surfaces". In: *NUWC Division Newport Technical Digest* (1995), pp. 65–71.
[16] Olivier Foin, Alain Berry, and Jeffrey Szabo. "Acoustic radiation from an elastic baffled rectangular plate covered by a decoupling coating and immersed in a heavy acoustic fluid". In: *The Journal of the Acoustical Society of America* 107.5 (2000), pp. 2501–2510.
[17] Meng Tao, Wei Lin Tang, and Hong Xing Hua. "Noise reduction analysis of an underwater decoupling layer". In: (2010).
[18] B Laulagnet and JL Guyader. "Sound radiation from a finite cylindrical shell covered with a compliant layer". In: (1991).
[19] Jie Deng et al. "Vibroacoustic mitigation for a cylindrical shell coupling with an acoustic black hole plate using Gaussian expansion component mode synthesis". In: *Composite Structures* 298 (2022), p. 116002.
[20] PC Jain, Abhijit Mukherjee, and Y Krishna. "Tuned mass dampers for flight vehicle components subjected to rocket noise". In: *Aerospace Science and Technology* 15.3 (2011), pp. 175–182.
[21] Bertrand J Brevart and Chris R Fuller. "Active control of coupled wave propagation in fluid-filled elastic cylindrical shells". In: *The journal of the Acoustical Society of America* 94.3 (1993), pp. 1467–1475.
[22] Yi Gu and Chris R Fuller. "Active control of sound radiation from a fluid-loaded rectangular uniform plate". In: *The Journal of the Acoustical Society of America* 93.1 (1993), pp. 337–345.
[23] Sheng Li. "Active modal control simulation of vibro-acoustic response of a fluid-loaded plate". In: *Journal of Sound and Vibration* 330.23 (2011), pp. 5545–5557.
[24] Daria Manushyna et al. "Application of vibroacoustic metamaterials for structural vibration reduction in space structures". In: *Mechanics Research Communications* 129 (2023), p. 104090.
[25] Fraunhofer Institute for Structural Durability and System Reliability LBF. *Silent Running — Vibroacoustic Metamaterials to Reduce Vibrations in Space Travel Applications*. https://www.lbf.fraunhofer.de/en/projects/silent-running-vibroacoustic-metamaterials.html. Accessed: 2024-08-22. 2024.
[26] Dah-You Maa. "Theory and design of microperforated panel sound-absorbing construction". In: *Scientia Sinica* 18 (1975), pp. 55–71.
[27] Dah-You Maa. "Theory of microslit absorbers". In: *Acta Acustica* 25 (2000), pp. 481–485.
[28] R.T. Randeberg. "Adjustable slitted panel absorber". In: *Acta Acustica* 88 (2002), pp. 507–512.
[29] W. Yang et al. "3D Printing of Polymeric Multi-Layer Micro-Perforated Panels for Tunable Wideband Sound Absorption". In: *Polymers* 12.2 (2020), p. 360.
[30] Kaufui V Wong and Aldo Hernandez. "A review of additive manufacturing." In: *ISRN mechanical engineering* (2012).
[31] Amit Bandyopadhyay and Susmita Bose. *Additive manufacturing*. CRC press, 2019.
[32] MacKenzie Brown and Paul Plaza. *A brief history of 3D printing: CAD crowd*. Jan. 2023. URL: https://www.cadcrowd.com/blog/a-brief-history-of-3d-printing/.

[33] Carl R. Deckard. "Selective laser sintering". PhD thesis. University of Texas, 1988.
[34] S. Scott Crump. *Apparatus and method for creating three-dimensional objects*. US Patent 5,121,329. June 1992.
[35] Dara G Schniederjans. "Adoption of 3D-printing technologies in manufacturing: A survey analysis". In: *International Journal of Production Economics* 183 (2017), pp. 287–298.
[36] James Norman et al. "A new chapter in pharmaceutical manufacturing: 3D-printed drug products". In: *Advanced drug delivery reviews* 108 (2017), pp. 39–50.
[37] Arianna De Mori et al. "3D printing and electrospinning of composite hydrogels for cartilage and bone tissue engineering". In: *Polymers* 10.3 (2018), p. 285.
[38] Yigong Liu et al. "Evaluating fabrication feasibility and biomedical application potential of in situ 3D printing technology". In: *Rapid Prototyping Journal* 22.6 (2016), pp. 947–955.
[39] Diana Popescu et al. "FDM process parameters influence over the mechanical properties of polymer specimens: A review". In: *Polymer Testing* 69 (2018), pp. 157–166. ISSN: 0142-9418. DOI: 10.1016/j.polymertesting.2018.05.020.
[40] Thomas G. Roberts. *Space Launch to Low Earth Orbit: How Much Does It Cost?* Accessed on May 31, 2023. 2022. URL: https://aerospace.csis.org/data/space-launch-to-low-earth-orbit-how-much-does-it-cost/.
[41] Melissa E. Orme et al. "Additive Manufacturing of Lightweight, Optimized, Metallic Components Suitable for Space Flight". In: *Journal of Spacecraft and Rockets* 54.5 (2017), pp. 1050–1059. DOI: 10.2514/1.A33749.
[42] Runze Huang et al. "Energy and emissions saving potential of additive manufacturing: the case of lightweight aircraft components". In: *Journal of Cleaner Production* 135 (2016), pp. 1559–1570. ISSN: 0959-6526. DOI: 10.1016/j.jclepro.2015.04.109.
[43] GE Additive. *Aviation and aerospace industry. GE Additive*. Accessed on May 31, 2023. 2022. URL: https://www.ge.com/additive/additive-manufacturing/industries/aviation-aerospace.
[44] Abdul Hai Alami et al. "Additive manufacturing in the aerospace and automotive industries: Recent trends and role in achieving sustainable development goals". In: *Ain Shams Engineering Journal* 14.11 (2023), p. 102516. ISSN: 2090-4479. DOI: 10.1016/j.asej.2023.102516.
[45] Mohammad Suhel Karkun and Sathish Dharmalingam. "3D printing technology in aerospace industry–a review". In: *International Journal of Aviation, Aeronautics, and Aerospace* 9.2 (2022), p. 4. DOI: 10.15394/ijaaa.2022.1708.
[46] *Aerospace 3D Printing Market by Offerings(Printers, Materials, Services, Software), Technology, Platform(Aircraft, UAVs, Spacecraft), Application(Prototyping, Tooling, Functional Parts), End Product, End User(OEM, MRO), & Region (2021-2026)*. Tech. rep. Markets and markets, 2021.
[47] Christo Dordlofva, Angelica Lindwall, and Peter Törlind. "Opportunities and Challenges for Additive Manufacturing in Space Applications". In: Aug. 2016. ISBN: 978-1-904670-80-3.
[48] Sunil C Joshi and Abdullah A Sheikh. "3D printing in aerospace and its long-term sustainability". In: *Virtual and physical prototyping* 10.4 (2015), pp. 175–185. DOI: 10.1080/17452759.2015.1111519.

[49] Jabil. *3D printing technology trends. A survey of manufacturing decision makers. Dimensional research.* 2021. URL: https://www.jabil.com/dam/jcr:82f12c7a-7475-42a0-a64f-0f4a625587d8/jabil-2021-3d-printing-tech-trends-report.pdf.

[50] P. Serlenga and F. Montaville. *Five questions to shape a winning 3-D printing strategy.* Tech. rep. Bain & Company, Inc., 2015.

[51] S. Touzé, M. Rauch, and JY. Hascoet. "Methodology for complexity and cost comparison between subtractive and additive manufacturing processes". In: *Journal of Intelligent Manufacturing* (2022). DOI: 10.1007/s10845-022-02059-z.

[52] A. Kausar. *Polymeric Nanocomposites with Carbonaceous Nanofillers for Aerospace Applications.* 1st. ISBN: 9780323996570. Elsevier, 2022.

[53] IEMAI. *The most airline-approved material–ultem 9085.* Accessed 16-08-2024. 2023. URL: https://www.iemai3d.com/index.php/the-most-airline-approved-material-high-performance-fdm-pei-thermoplastic/.

[54] STRATASYS. *ULTEM™ 1010 resin.* Accessed 16-08-2024. URL: https://support.stratasys.com/en/Materials/FDM/ULTEM%E2%84%A2-1010-resin.

[55] Max Kandula. "Broadband shock noise reduction in turbulent jets by water injection". In: *Applied Acoustics* 70.7 (2009), pp. 1009–1014.

[56] Caroline P Lubert, Kent L Gee, and Seiji Tsutsumi. "Supersonic jet noise from launch vehicles: 50 years since NASA SP-8072". In: *The Journal of the Acoustical Society of America* 151.2 (2022), pp. 752–791.

[57] Roberto Garcia. *Assessment of microphone phased array for measuring launch vehicle lift-off acoustics.* Tech. rep. 2012.

[58] P Malbéqui, R Davy, and C Bresson. "Experimental characterization of the acoustics of the future Ariane 6 launch pad". In: *7th European Conference for Aeronautics and Space Sciences, Milan, Italy.* 2017.

[59] R Picó et al. "Acoustic behavior of the VEGA launch pad environment". In: *Proceedings of EuroRegio* (2016), pp. 13–15.

[60] Daniel Allgood, Grady Saunders, and Lester Langford. "Reduction of altitude diffuser jet noise using water injection". In: *50th AIAA Aerospace Sciences Meeting including the New Horizons Forum and Aerospace Exposition.* 2012, p. 680.

[61] Hwayoung Oh et al. "Numerical study for flame deflector design of a space launch vehicle". In: *Advances in Space Research* 59.7 (2017), pp. 1833–1847. ISSN: 0273-1177. DOI: https://doi.org/10.1016/j.asr.2016.12.038.

[62] Seiji Tsutsumi et al. "Generation and propagation of pressure waves from H-IIA launch vehicle at lift-off". In: *46th AIAA aerospace sciences meeting and exhibit.* 2008, p. 390.

[63] D Gely et al. "Reduction of supersonic jet noise-application to the Ariane 5 launch vehicle". In: *6th Aeroacoustics Conference and Exhibit.* 2000, p. 2026.

[64] DA Bond. *A Summary of Model and Full-Scale Acoustic Data for Prediction of Missile Lift-Off Noise Environments. Rept.* Tech. rep. NOR-64-215, Northrop Corp, 1964.

[65] Chenglong Xing et al. "Numerical investigations on acoustic environment of multi-nozzle launch vehicle at lift-off". In: *Aerospace Science and Technology* 106 (2020), p. 106140.

[66] Vincenzo D'Alessandro et al. "A review of the vibroacoustics of sandwich panels: Models and experiments". In: *Journal of Sandwich Structures & Materials* 15.5 (2013), pp. 541–582.

[67] K.U. Ingard. *Notes on Sound Absorption Technology*. Notebook. Noise Control Foundation, 1994. ISBN: 9780931784286. URL: https://books.google.es/books?id=FTnvAAAACAAJ.

[68] Jorge P Arenas and Malcolm J Crocker. "Recent trends in porous sound-absorbing materials". In: *Sound & vibration* 44.7 (2010), pp. 12–18.

[69] Michael E Delany and EN Bazley. "Acoustical properties of fibrous absorbent materials". In: *Applied acoustics* 3.2 (1970), pp. 105–116.

[70] Pedro Cobo and Francisco Simón. "Multiple-layer microperforated panels as sound absorbers in buildings: a review". In: *Buildings* 9.2 (2019), p. 53.

[71] Bert Phillips, Ned P. Hannum, and Louis M. Russel. *On the design of acoustic liners for rocket engines: Helmholtz resonators evaluated with a rocket combustor*. Tech. rep. National Aeronautics and Space Administration, 1969.

[72] Dah-You Maa. "Potential of microperforated panel absorber". In: *The Journal of the Acoustical Society of America* 104.5 (1998), pp. 2861–2866.

[73] J.F. Allard. *Propagation of Sound in Porous Media: Modelling Sound Absorbing Materials*. London: Elsevier, 1993.

[74] Jean Allard and Noureddine Atalla. *Propagation of sound in porous media: modelling sound absorbing materials*. John Wiley & Sons, 2009.

[75] N. Atalla and F. Sgard. "Modelling of perforated plates and screens using rigid frame porous models". In: *Journal of Sound and Vibration* 303 (2007), pp. 195–208.

[76] C. Zwikker and C.W. Kosten. *Sound Absorbing Materials*. New York: Elsevier, 1949.

[77] I. Crandall. *Theory of Vibrating Systems and Sound*. New York: D. Van Nostrand Company, 1926.

[78] Uno Ingard. "On the theory and design of acoustic resonators". In: *The Journal of the acoustical society of America* 25.6 (1953), pp. 1037–1061.

[79] John William Strutt Rayleigh. *The theory of sound*. Vol. 1. Macmillan, 1877.

[80] Pedro Cobo. "Modelling of microperforated panel absorbers with circular and slit hole geometries". In: *Acoustics*. Vol. 3. 4. MDPI. 2021, pp. 665–678.

[81] Perforated panel absorbers with viscous energy dissipation enhanced by orifice design. "Randeberg, Rolf Tore". PhD thesis. Norweian University of Science and Technology, Trondheim, Norway, 2000.

[82] Tor Erik Vigran and Okø Pettersen. "The absorption of slotted panels revisited". In: *Proceedings of the Forum Acusticum*. 2005, pp. 1245–1322.

[83] Jaime Pfretzschner et al. "Microperforated insertion units: An alternative strategy to design microperforated panels". In: *Applied Acoustics* 67.1 (2006), pp. 62–73.

[84] Heidi Ruiz et al. "Acoustic properties of plates with unevenly distributed macroperforations backed by woven meshes". In: *The journal of the acoustical society of America* 132.5 (2012), pp. 3138–3147.

[85] S. Huang et al. "Micro-perforated absorbers with incompletely partitioned cavities". In: *Applied Acoustics* 126 (2017), pp. 114–119.

[86] A. Mosa et al. "Theoretical model of absorption coefficient of an inhomogeneous MPP absorber with multi-cavity depths". In: *Applied Acoustics* 146 (2019), pp. 409–419.

[87] Dah-You Maa. "Microperforated-panel wideband absorbers". In: *Noise control engineering journal* 29.3 (1987), pp. 77–84.

[88] Jinkyo Lee and George W Swenson. "Compact sound absorbers for low frequencies". In: *Noise Control Engineering Journal* 38.3 (1992), pp. 109–117.

[89] DH Lee and YP Kwon. "Estimation of the absorption performance of multiple layer perforated panel systems by transfer matrix method". In: *Journal of sound and vibration* 278.4-5 (2004), pp. 847–860.

[90] Pedro Cobo et al. "Comparison of models describing double layer microperforated absorbers". In: *Noise Control Engineering Journal* 57.1 (2009), pp. 54–63.

[91] Pedro Cobo et al. "A wideband triple-layer microperforated panel sound absorber". In: *Composite Structures* 226 (2019), p. 111220.

[92] S.H. Park. "Acoustic properties of micro-perforated panel absorbers backed by Helmholtz resonators for the improvement of low-frequency sound absorption". In: *Journal of Sound and Vibration* 332.20 (2013), pp. 4895–4911.

[93] Xiao-Ling Gai et al. "Experimental study on sound absorption performance of microperforated panel with membrane cell". In: *Applied Acoustics* 110 (2016), pp. 241–247.

[94] XH Duan et al. "Sound absorption of a flexible micro-perforated panel absorber based on PVDF piezoelectric film". In: *Applied Acoustics* 88 (2015), pp. 84–89.

[95] Wencheng Guo and Hequn Min. "A compound micro-perforated panel sound absorber with partitioned cavities of different depths". In: *Energy Procedia* 78 (2015), pp. 1617–1622.

[96] YJ Qian et al. "Improvement of sound absorption characteristics under low frequency for micro-perforated panel absorbers using super-aligned carbon nanotube arrays". In: *Applied acoustics* 82 (2014), pp. 23–27.

[97] Xiaodan Zhao and Xiangqian Fan. "Enhancing low frequency sound absorption of micro-perforated panel absorbers by using mechanical impedance plates". In: *Applied Acoustics* 88 (2015), pp. 123–128.

[98] Xiao-dan Zhao, Xin Wang, and Yong-jie Yu. "Enhancing low-frequency sound absorption of micro-perforated panel absorbers by combining parallel mechanical impedance". In: *Applied Acoustics* 130 (2018), pp. 300–304.

[99] Bo-Seung Kim et al. "Sound absorption structure in helical shapes made using fibrous paper". In: *Composite Structures* 134 (2015), pp. 90–94.

[100] Bo-Seung Kim et al. "Experimental study for improving sound absorption of a composite helical-shaped porous structure using carbon fiber". In: *Composite Structures* 145 (2016), pp. 242–247.

[101] YJ Qian et al. "Investigation on micro-perforated panel absorber with ultra-micro perforations". In: *Applied Acoustics* 74.7 (2013), pp. 931–935.

[102] Pedro Cobo and Francisco Montero de Espinosa. "Proposal of cheap microperforated panel absorbers manufactured by infiltration". In: *Applied acoustics* 74.9 (2013), pp. 1069–1075.

[103] Z. Liu et al. "Acoustic measurement of a 3D printed microperforated panel combined with porous material". In: *Measurement* 104 (2017), pp. 233–236.

[104] C. Jiang et al. "Acoustic Absorption of Porous Materials Produced by Additive Manufacturing with Varying Geometries". In: *Proceedings of Acoustics*. 2017.

[105] D. Akiwate. "Acoustic characterization of additive manufactured perforated panel backed by honeycomb structure with circular and non-circular perforations". In: *Applied Acoustics* 155 (2017), pp. 271–279.

[106] HT Shi et al. "Vibration isolation methods in spacecraft: a review of current techniques". In: *Advances in Space Research* 73.8 (2024), pp. 3993–4023.

[107] Chao Qin et al. "Design and optimization of the micro-vibration isolation system for large space telescope". In: *Journal of Sound and Vibration* 482 (2020), p. 115461.

[108] Sudhir Kaul. "Vibration isolation—background". In: *Modeling and Analysis of Passive Vibration Isolation Systems, Elsevier* (2021), pp. 1–26.

[109] M Safarabadi, H Haghshenas, and H Kelardeh. "Design of micro-vibration isolation system for a remote-sensing satellite payload using viscoelastic Materials". In: *Eng. Solid Mech* 8 (2020), pp. 69–76.

[110] Changcheng Deng et al. "Effects of rubber shock absorber on the flywheel micro vibration in the satellite imaging system". In: *Photonic Sensors* 6 (2016), pp. 372–384.

[111] Haitao Luo et al. "Design and experiment of micro-vibration isolation system for optical satellite". In: *European Journal of Mechanics-A/Solids* 97 (2023), p. 104833.

[112] BJ Kawak, BH Cabon, and GS Aglietti. "Innovative viscoelastic material selection strategy based on dma and mini-shaker tests for spacecraft applications". In: *Acta Astronautica* 131 (2017), pp. 18–27.

[113] Shenghao Shi, Dongxu Li, and Qing Luo. "Design and dynamic analysis of micro-vibration isolator for Single Gimbal Control Moment Gyro". In: *Procedia Engineering* 99 (2015), pp. 551–559.

[114] Chao Xu et al. "Modeling and analysis of a viscoelastic micro-vibration isolation and mitigation platform for spacecraft". In: *Journal of Vibration and Control* 24.18 (2018), pp. 4337–4352.

[115] SN Sayapin and Yu N Artemenko. "Intelligence system for active vibration isolation and pointing of ultrahigh-precision large space structures in real time". In: *Smart Electromechanical Systems* (2016), pp. 103–115.

[116] Jie Huang, Juntong Xi, and Zif Yu. "Study on micro-vibration isolation system design and validation for the SDLT-1 satellite of China". In: *Journal of Vibration Engineering & Technologies* 11.8 (2023), pp. 3879–3891.

[117] Xi Wang, Haomin Wu, and Bintang Yang. "Micro-vibration suppressing using electromagnetic absorber and magnetostrictive isolator combined platform". In: *Mechanical Systems and Signal Processing* 139 (2020), p. 106606.

[118] Ze-Qi Lu et al. "Vibration isolation and energy harvesting integrated in a Stewart platform with high static and low dynamic stiffness". In: *Applied Mathematical Modelling* 89 (2021), pp. 249–267.

[119] Jie Tang et al. "A 6-DOF micro-vibration isolation platform based on the quasi-zero-stiffness isolator". In: *Proceedings of the Institution of Mechanical Engineers, Part C: Journal of Mechanical Engineering Science* 235.22 (2021), pp. 6019–6035.

[120] Chuan Li et al. "The Chinese Hα solar explorer (CHASE) mission: An overview". In: *Science China Physics, Mechanics & Astronomy* 65.8 (2022), p. 289602.

[121] Yuyang Chai, Jing Bian, and Meng Li. "A novel quasi-zero-stiffness isolation platform via tunable positive and negative stiffness compensation mechanism". In: *Nonlinear Dynamics* 112.1 (2024), pp. 101–123.

[122] Cheng Fang et al. "Rocking bridge piers equipped with shape memory alloy (SMA) washer springs". In: *Engineering Structures* 214 (2020), p. 110651.

[123] Jiadeng Wang et al. "Performance of a launch isolator: Theoretical and experimental study". In: *Journal of Sound and Vibration* 483 (2020), p. 115487.

[124] Seong-Cheol Kwon, Su-Hyeon Jeon, and Hyun-Ung Oh. "Performance evaluation of spaceborne cryocooler micro-vibration isolation system employing pseudoelastic SMA mesh washer". In: *Cryogenics* 67 (2015), pp. 19–27.

[125] Seong-Cheol Kwon, Yeon-Hyeok Park, and Hyun-Ung Oh. "Characteristics of spaceborne cooler vibration isolator using a pseudoelastic shape memory alloy". In: *Sensors and Smart Structures Technologies for Civil, Mechanical, and Aerospace Systems 2017*. Vol. 10168. SPIE. 2017, pp. 696–702.

[126] JC Ji, Quantian Luo, and Kan Ye. "Vibration control based metamaterials and origami structures: a state-of-the-art review". In: *Mechanical Systems and Signal Processing* 161 (2021), p. 107945.

[127] Zhangming Wu et al. "A novel design of vibration isolator with high and frequency dependent damping characteristics based on a Large Negative Poisson's Ratio (LNPR) structure". In: *Mechanical Systems and Signal Processing* 186 (2023), p. 109818.

[128] Chao Xu et al. "Modeling and analysis of a viscoelastic micro-vibration isolation and mitigation platform for spacecraft". In: *Journal of Vibration and Control* 24.18 (2018), pp. 4337–4352.

[129] Ze-Qi Lu et al. "A dual-functional metamaterial for integrated vibration isolation and energy harvesting". In: *Journal of Sound and Vibration* 509 (2021), p. 116251.

[130] Chunchuan Liu et al. "Recent advances in micro-vibration isolation". In: *Mechanical Systems and Signal Processing* 56 (2015), pp. 55–80.

[131] Kyung-min Lee. "Design and analysis of a vertically moving voice coil motor with gravity compensation for semiconductor equipment". In: *Sensors and Actuators A: Physical* 344 (2022), p. 113735.

[132] Jie Tang et al. "Design and experimental study of a VCM-based whole-spacecraft vibration isolation system". In: *Journal of Aerospace Engineering* 31.5 (2018), p. 04018045.

[133] Weichao Chi, Dengqing Cao, and Wenhu Huang. "Design of active whole-spacecraft vibration isolation based on voice-coil motor". In: *Sensors and Smart Structures Technologies for Civil, Mechanical, and Aerospace Systems 2014*. Vol. 9061. SPIE. 2014, pp. 1041–1047.

[134] Weipeng Li et al. "Design and experiments of an active isolator for satellite micro-vibration". In: *Chinese Journal of Aeronautics* 27.6 (2014), pp. 1461–1468.

[135] Barış Can Yalçın and Kadir Erkan. "3-DoF zero power micro vibration isolation via linear matrix inequalities based on H and H2 control approaches". In: *Mechanical Systems and Signal Processing* 153 (2021), p. 107506.

[136] Wei Liu et al. "Control performance simulation and tests for microgravity active vibration isolation system onboard the Tianzhou-1 cargo spacecraft". In: *Astrodynamics* 2 (2018), pp. 339–360.

[137] Frédéric Giraud and Christophe Giraud-Audine. "Chapter One - Introduction". In: *Piezoelectric Actuators: Vector Control Method*. Ed. by Frédéric Giraud and Christophe Giraud-Audine. Butterworth-Heinemann, 2019, pp. 1–42. ISBN: 978-0-12-814186-1.

DOI: https://doi.org/10.1016/B978-0-12-814186-1.00005-3. URL: https://www.sciencedirect.com/science/article/pii/B9780128141861000053.

[138] Peng Zhang. "Chapter 3 - Sensors and actuators". In: *Advanced Industrial Control Technology*. Ed. by Peng Zhang. Oxford: William Andrew Publishing, 2010, pp. 73–116. ISBN: 978-1-4377-7807-6. DOI: https://doi.org/10.1016/B978-1-4377-7807-6.10003-8. URL: https://www.sciencedirect.com/science/article/pii/B9781437778076100038.

[139] Yeon-Hyeok Park et al. "High damping passive launch vibration isolation system using superelastic SMA with multilayered viscous lamina". In: *Aerospace* 8.8 (2021), p. 201.

[140] Mou Li et al. "The pointing and vibration isolation integrated control method for optical payload". In: *Journal of Sound and Vibration* 438 (2019), pp. 441–456.

[141] Francesco Braghin, Simone Cinquemani, and Ferruccio Resta. "A model of magnetostrictive actuators for active vibration control". In: *Sensors and Actuators A: physical* 165.2 (2011), pp. 342–350.

[142] Lei Zhou and Jingjie Wu. "Magnetic levitation technology for precision motion systems: A review and future perspectives". In: *International Journal of Automation Technology* 16.4 (2022), pp. 386–402.

[143] Zhaopei Gong et al. "Design and control of a novel six-DOF maglev platform for positioning and vibration isolation". In: *2017 2nd International Conference on Advanced Robotics and Mechatronics (ICARM)*. IEEE. 2017, pp. 155–160.

[144] Ye-Wei Zhang et al. "Integration of a nonlinear vibration absorber and levitation magnetoelectric energy harvester for whole-spacecraft systems". In: *Acta Mechanica Solida Sinica* 32 (2019), pp. 298–309.

[145] Wei Liu et al. "Flight test results of the microgravity active vibration isolation system in China's Tianzhou-1 mission". In: *Microgravity Science and Technology* 30 (2018), pp. 995–1009.

[146] LI Lin et al. "Image motion and experimental study of a 0.1 space pointing measuring instrument for micro-vibration conditions". In: *Chinese Journal of Aeronautics* 36.2 (2023), pp. 191–200.

[147] Xiaobo Tan and John S. Baras. "Modeling and control of hysteresis in magnetostrictive actuators". In: *Automatica* 40.9 (2004), pp. 1469–1480. ISSN: 0005-1098. DOI: https://doi.org/10.1016/j.automatica.2004.04.006.

[148] Kadir Erkan and Takafumi Koseki. "Fuzzy model-based monlinear maglev control for active vibration control systems". In: *International Journal of Applied Electromagnetics and Mechanics* 25.1-4 (2007), pp. 543–548.

[149] Luis Suárez and Manuel Domínguez. "Sustainability and environmental impact of fused deposition modelling (FDM) technologies". In: *The International Journal of Advanced Manufacturing Technology* 106 (2020), pp. 1267–1279.

[150] Pavan Kumar Gurrala and Srinivasa Prakash Regalla. "Optimization of support material and build time in fused deposition modeling (FDM)". In: *Applied Mechanics and Materials* 110 (2012), pp. 2245–2251.

[151] Marlon Wesley Machado Cunico. "Study and optimization of FDM process parameters for support-material-free deposition of filaments and increased layer adherence: This paper investigates control factors and process parameters that allow the fabrication

of negative surface features without a support material". In: *Virtual and Physical Prototyping* 8.2 (2013), pp. 127–134.

[152] Kim Ragaert, Laurens Delva, and Kevin Van Geem. "Mechanical and chemical recycling of solid plastic waste". In: *Waste management* 69 (2017), pp. 24–58.

[153] Li Shen and Ernst Worrell. "Plastic recycling". In: *Handbook of recycling*. Elsevier, 2024, pp. 497–510.

[154] Mohammed Nuwaid Nattukallingal, Ziying Ran, and Ahmed Abass. "A Material-Recycling Unit for the Fused Deposition Modelling of Three-Dimensional Printing Systems". In: *Applied Sciences* 13.13 (2023), p. 7515.

[155] Ralf Zgeib et al. "Development of a low-cost quad-extrusion 3D bioprinting system for multi-material tissue constructs". In: *International Journal of Bioprinting* 10.1 (2023), p. 0159.

[156] Tobias Hullete. *Direct Drive vs Bowden Extruder: The Differences*. Accessed: 2024-09-17. 2024. URL: https://all3dp.com/2/direct-vs-bowden-extruder-technology-shootout/.

[157] Pooyan Nayyeri, Kourosh Zareinia, and Habiba Bougherara. "Planar and nonplanar slicing algorithms for fused deposition modeling technology: A critical review". In: *The International Journal of Advanced Manufacturing Technology* 119.5 (2022), pp. 2785–2810.

[158] Michael Wüthrich et al. "A novel slicing strategy to print overhangs without support material". In: *Applied Sciences* 11.18 (2021), p. 8760.

[159] Federico Insero, Valentina Furlan, and Hermes Giberti. "Non-planar slicing for filled free-form geometries in robot-based FDM". In: *Journal of Intelligent Manufacturing* (2023), pp. 1–19.

[160] Lukas Pelzer and Christian Hopmann. "Additive manufacturing of non-planar layers with variable layer height". In: *Additive Manufacturing* 37 (2021), p. 101697.

[161] Van-Nam Hoang et al. "Adaptive concurrent topology optimization of coated structures with nonperiodic infill for additive manufacturing". In: *Computer-Aided Design* 129 (2020), p. 102918.

[162] WQ Hao et al. "A physics-informed machine learning approach for notch fatigue evaluation of alloys used in aerospace". In: *International Journal of Fatigue* 170 (2023), p. 107536.

[163] Nikolaos Kolokas et al. "A generic fault prognostics algorithm for manufacturing industries using unsupervised machine learning classifiers". In: *Simulation Modelling Practice and Theory* 103 (2020), p. 102109.

[164] Devara Venkata Krishna and Mamilla Ravi Sankar. "Machine learning-assisted extrusion-based 3D Bioprinting for tissue regeneration applications". In: *Annals of 3D Printed Medicine* (2023), p. 100132.

[165] Bonsa Regassa Hunde and Abraham Debebe Woldeyohannes. "Future prospects of computer-aided design (CAD)–A review from the perspective of artificial intelligence (AI), extended reality, and 3D printing". In: *Results in Engineering* 14 (2022), p. 100478.

[166] Guo Dong Goh and Wai Yee Yeong. "Applications of machine learning in 3D printing". In: *Materials Today: Proceedings* 70 (2022), pp. 95–100.

[167] Guo Dong Goh, Nur Muizzu Bin Hamzah, and Wai Yee Yeong. "Anomaly detection in fused filament fabrication using machine learning". In: *3D Printing and Additive Manufacturing* 10.3 (2023), pp. 428–437.

[168] Evangelos Tyflopoulos and Martin Steinert. "A comparative study of the application of different commercial software for topology optimization". In: *Applied Sciences* 12.2 (2022), p. 611.

[169] Sai Nithin Reddy et al. "Topology optimization software for additive manufacturing: A review of current capabilities and a real-world example". In: *ASME 2016 International Design Engineering Technical Conferences and Computers and Information in Engineering Conference, IDETC/CIE 2016*. American Society of Mechanical Engineers (ASME). 2016.

[170] Mirko Kariž et al. "Effect of sanding and plasma treatment of 3D-printed parts on bonding to wood with PVAc adhesive". In: *Polymers* 13.8 (2021), p. 1211.

[171] Jure Žigon, Mirko Kariž, and Matjaž Pavlič. "Surface finishing of 3D-printed polymers with selected coatings". In: *Polymers* 12.12 (2020), p. 2797.

[172] Weijie Li et al. "Influence of sanding and plasma treatment on shear bond strength of 3D-printed PEI, PEEK and PEEK/CF". In: *International Journal of Adhesion and Adhesives* 100 (2020), p. 102614.

[173] N Jayanth, P Senthil, and C Prakash. "Effect of chemical treatment on tensile strength and surface roughness of 3D-printed ABS using the FDM process". In: *Virtual and Physical Prototyping* 13.3 (2018), pp. 155–163.

[174] Andrea Pearse. "Chemical Smoothing of 3D Printed ABS". MA thesis. University of Cope Town, 2018.

[175] Clayton Neff, Matthew Trapuzzano, and Nathan B Crane. "Impact of vapor polishing on surface roughness and mechanical properties for 3D printed ABS". In: (2016).

[176] Brian Jumaquio Tuazon, Michaela Tayag Espino, and John Ryan Cortez Dizon. "Investigation on the effects of acetone vapor-polishing to fracture behavior of abs printed materials at different operating temperature". In: *Materials Science Forum*. Vol. 1005. Trans Tech Publ. 2020, pp. 141–149.

[177] KA Lorenz et al. "A review of hybrid manufacturing". In: (2015).

[178] Zicheng Zhu et al. "A review of hybrid manufacturing processes–state of the art and future perspectives". In: *International Journal of Computer Integrated Manufacturing* 26.7 (2013), pp. 596–615.

[179] C Al Christopher et al. "High performance polymers for oil and gas applications". In: *Reactive and Functional Polymers* 162 (2021), p. 104878.

[180] Linda Sawyer, David T Grubb, and Gregory F Meyers. *Polymer microscopy*. Springer Science & Business Media, 2008.

[181] Matthias Wagner. *Thermal analysis in practice: fundamental aspects*. Carl Hanser Verlag GmbH Co KG, 2017.

[182] Paul M Hergenrother. "The use, design, synthesis, and properties of high performance/high temperature polymers: an overview". In: *High Performance Polymers* 15.1 (2003), pp. 3–45.

[183] Michel Biron. "2 - Thermoplastic Specific Properties". In: *Material Selection for Thermoplastic Parts*. Ed. by Michel Biron. Oxford: William Andrew Publishing, 2016,

pp. 39–75. ISBN: 978-0-7020-6284-1. DOI: https://doi.org/10.1016/B978-0-7020-6284-1.00002-7.

[184] Anshuman Shrivastava. "1 - Introduction to Plastics Engineering". In: *Introduction to Plastics Engineering*. Ed. by Anshuman Shrivastava. Plastics Design Library. William Andrew Publishing, 2018, pp. 1–16. ISBN: 978-0-323-39500-7. DOI: https://doi.org/10.1016/B978-0-323-39500-7.00001-0.

[185] Dries Vaes and Peter Van Puyvelde. "Semi-crystalline feedstock for filament-based 3D printing of polymers". In: *Progress in Polymer Science* 118 (2021), p. 101411. ISSN: 0079-6700. DOI: https://doi.org/10.1016/j.progpolymsci.2021.101411.

[186] Hui Quan et al. "On transcrystallinity in semi-crystalline polymer composites". In: *Composites Science and Technology* 65.7-8 (2005), pp. 999–1021.

[187] Joseph P. Greene. "8 - Engineering Plastics". In: *Automotive Plastics and Composites*. Ed. by Joseph P. Greene. Plastics Design Library. William Andrew Publishing, 2021, pp. 107–125. ISBN: 978-0-12-818008-2. DOI: https://doi.org/10.1016/B978-0-12-818008-2.00022-2.

[188] Yao Ji et al. "Progress of liquid crystal polyester (LCP) for 5G application". In: *Advanced Industrial and Engineering Polymer Research* 3.4 (2020), pp. 160–174. ISSN: 2542-5048. DOI: https://doi.org/10.1016/j.aiepr.2020.10.005.

[189] Laurence W. McKeen. *5 - Polyesters*. Ed. by Laurence W. McKeen. Fourth Edition. Plastics Design Library. William Andrew Publishing, 2019, pp. 125–165. ISBN: 978-0-12-816457-0. DOI: https://doi.org/10.1016/B978-0-12-816457-0.00005-8.

[190] Edward N. Peters and R.K. Arisman. *Engineering thermoplastics*. Elsevier, New York, 2000.

[191] SABIC. *ULTEM® Resin - Family of High Heat Solutions*. Accessed: 2024-08-22. 2024. URL: https://www.sabic.com/en/products/specialties/ultem-resin-family-of-high-heat-solutions/ultem-resin.

[192] Maleka P Hashmi and Trever M Koester. "Applications of synthetically produced materials in clinical medicine". In: (2018).

[193] I William Serfaty. "Polyetherimide". In: *Engineering Thermoplastics*. CRC Press, 2020, pp. 283–297.

[194] STRATASYS. *UTC Aerospace Systems improves production with 3D printing*. Accessed 16-08-2024. 2020. URL: https://www.stratasys.com/mx/resources/case-studies/utc/.

[195] *Frequently Asked Questions: ULTEM™ 9085*. Tech. rep. STRATASYS, 2022.

[196] Suchart Siengchin. "A review on lightweight materials for defence applications: Present and future developments". In: *Defence Technology* 24 (2023), pp. 1–17.

[197] Mingzong Zhang, Phillip Choi, and Uttandaraman Sundararaj. "Molecular dynamics and thermal analysis study of anomalous thermodynamic behavior of poly (ether imide)/polycarbonate blends". In: *Polymer* 44.6 (2003), pp. 1979–1986.

[198] A Zabaleta et al. "Rubber toughening of poly (ether imide) by modification with poly (butylene terephthalate)". In: *European polymer journal* 45.2 (2009), pp. 466–473.

[199] ST Amancio-Filho et al. "Thermal degradation of polyetherimide joined by friction riveting (FricRiveting). Part I: Influence of rotation speed". In: *Polymer degradation and stability* 93.8 (2008), pp. 1529–1538.

[200] David González-Bárcena et al. “HERCCULES: A university balloon-borne experiment for BEXUS 32 to characterize the thermal environment in the stratosphere using COTS”. In: *Acta Astronautica* 220 (2024), pp. 305–320. ISSN: 0094-5765. DOI: https://doi.org/10.1016/j.actaastro.2024.04.034.

[201] B. Boado-Cuartero et al. “Design of a COTS-based, Low-cost, Electronic Box to Standardize Student Balloon Applications”. In: *IEEE Aerospace and Electronic Systems Magazine* (2025), pp. 1–12. DOI: 10.1109/MAES.2025.3577143.

[202] Krishna P. Motaparti et al. “Experimental investigation of effects of build parameters on flexural properties in fused deposition modelling parts”. In: *Virtual and Physical Prototyping* 12.3 (2017), pp. 207–220. DOI: 10.1080/17452759.2017.1314117.

[203] Jikai Liu et al. “Current and future trends in topology optimization for additive manufacturing”. In: *Structural and Multidisciplinary Optimization* 57 (2018), pp. 2457–2483. DOI: 10.1007/s00158-018-1994-3.

[204] Guo Dong Goh et al. “Process–structure–properties in polymer additive manufacturing via material extrusion: A review”. In: *Critical Reviews in Solid State and Materials Sciences* 45.2 (2020), pp. 113–133. DOI: 10.1080/10408436.2018.1549977.

[205] John J Laureto and Joshua M Pearce. “Anisotropic mechanical property variance between ASTM D638-14 type i and type iv fused filament fabricated specimens”. In: *Polymer Testing* 68 (2018), pp. 294–301. DOI: 10.1016/j.polymertesting.2018.04.029.

[206] *ASTM D638-22: Standard Test Method for Tensile Properties of Plastics*. Standard. ASTM International, 2022.

[207] Enrique Cuan-Urquizo et al. “Characterization of the mechanical properties of FFF structures and materials: A review on the experimental, computational and theoretical approaches”. In: *Materials* 12.6 (2019), p. 895. DOI: 10.3390/ma12060895.

[208] Blanca Boado Cuartero, Javier Pérez-Álvarez, and Elena Roibás Millán. “Variation of Mechanical Properties of ULTEM™ 9085 and 1010 Depending on Orientation and Printing Direction”. In: *International conference on The Digital Transformation in the Graphic Engineering*. Springer. 2023, pp. 801–813. DOI: 10.1007/978-3-031-51623-8_80.

[209] Blanca Boado-Cuartero, Javier Pérez-Álvarez, and Elena Roibás-Millán. “Material Characterization of High-Performance Polymers for Additive Manufacturing (AM) in Aerospace Mechanical Design”. In: *Aerospace* 11.9 (2024), p. 748. DOI: 10.3390/aerospace11090748.

[210] *Plastics – Determination of tensile properties*. Standard. International Organization for Standardization, 2019.

[211] *Plastics – Determination of flexural properties*. Standard. International Organization for Standardization, 2019.

[212] *Plastics — Determination of compressive properties*. Standard. International Organization for Standardization, 2002.

[213] *Standard Test Method for Compressive Properties of Rigid Plastics*. Standard. ASTM International, 2002.

[214] *ASTM D6110-10 Standard Test Method for Determining the Charpy Impact Resistance of Notched Specimens of Plastics*. Standard. ASTM International, 2010.

[215] *Plastics – Determination of Charpy impact properties – Part 1: Non-instrumented impact test*. Standard. International Organization for Standardization, 2010.
[216] *ULTEM™ 9085 resin. FDM©Thermoplastic Filament*. Tech. rep. Stratasys, 2021.
[217] *ULTEM™ 1010 resin. FDM©Thermoplastic Filament*. Tech. rep. Stratasys, 2020.
[218] *CAMPUS ©, ULTEM™ 1010 Resin, 2022*. Tech. rep. CAMPUS, 2022.
[219] *PEI ULTEM™ 9085 Resin, 2021*. Tech. rep. MCPP, 2021.
[220] *Materials Testing Procedure*. Tech. rep. STRATASYS, 2019.
[221] *ASTM D638 Tensile Properties of Plastics*. Standard. ASTM International, 2010.
[222] *ASTM D790-17 Standard Test Methods for Flexural Properties of Unreinforced and Reinforced Plastics and Electrical Insulating Materials*. Standard. ASTM International, 2017.
[223] Elisa Padovano et al. "Mechanical and thermal behavior of ultem® 9085 fabricated by fused-deposition modeling". In: *Applied Sciences* 10.9 (2020), p. 3170. DOI: 10.3390/app10093170.
[224] Brian W Kaplun et al. "Influence of orientation on mechanical properties for high-performance fused filament fabricated ultem 9085 and electro-statically dissipative polyetherketoneketone". In: *Additive Manufacturing* 36 (2020), p. 101527. DOI: 10.1016/j.addma.2020.101527.
[225] RJ Zaldivar et al. "Influence of processing and orientation print effects on the mechanical and thermal behavior of 3D-Printed ULTEM® 9085 Material". In: *Additive Manufacturing* 13 (2017), pp. 71–80. DOI: 10.1016/j.addma.2016.11.007.
[226] Chrysoula Pandelidi et al. "Parametric study on tensile and flexural properties of ULTEM 1010 specimens fabricated via FDM". In: *Rapid Prototyping Journal* 27.2 (2021), pp. 429–451. DOI: 10.1108/RPJ-10-2019-0274.
[227] Kate Iren Byberg, Aboma Wagari Gebisa, and Hirpa G Lemu. "Mechanical properties of ULTEM 9085 material processed by fused deposition modeling". In: *Polymer Testing* 72 (2018), pp. 335–347. DOI: 10.1016/j.polymertesting.2018.10.040.
[228] Gregory Taylor et al. "Flexural behavior of additively manufactured Ultem 1010: experiment and simulation". In: *Rapid Prototyping Journal* 24.6 (2018), pp. 1003–1011. DOI: 10.1108/RPJ-02-2018-0037.
[229] K.P. Motaparti et al. "Effects of build parameters on compression properties for ULTEM™ 9085 parts by fused deposition modelling." In: *Solid Freeform Fabrication 2016: Proceedings of the 27th Annual International Solid Freeform Fabrication Symposium - An Additive Manufacturing Conference*. Austin, TX., 2016.
[230] Xue Wang et al. "Effect of Porosity on Mechanical Properties of 3D Printed Polymers: Experiments and Micromechanical Modeling Based on X-ray Computed Tomography Analysis". In: *Polymers* 11.7 (2019). ISSN: 2073-4360. DOI: 10.3390/polym11071154.
[231] Ahmad Y. Al-Maharma1, Sandeep P. Patil1, and Bernd Markert1. "Effects of porosity on the mechanical properties of additively manufactured components: a critical review". In: *Materials Research Express* 7.12 (2020). DOI: 10.1088/2053-1591/abcc5d.
[232] Eugene Jahnke and Fritz Emde. *Tables of Functions: With Formulae and Curves*. Dover Publications Inc., 1945.
[233] Thomas Henry Melling. "The acoustic impendance of perforates at medium and high sound pressure levels". In: *Journal of Sound and Vibration* 29.1 (1973), pp. 1–65.

[234] Sergei Nikolaevich Rzhevkin. *A Course of Lectures on the Theory of Sound*. London, UK: Pergamon Press, 1963.

[235] Hasan Koruk and Garip Genç. "Acoustic and mechanical properties of luffa fiber-reinforced biocomposites". In: *Mechanical and physical testing of biocomposites, fibre-reinforced composites and hybrid composites*. Elsevier, 2019, pp. 325–341.

[236] *Acoustics – Determination of sound absorption coefficient and impedance in impedance tubes*. Standard. International Organization for Standardization, 1996.

[237] *ASTM E1050-19: Standard Test Method for Impedance and Absorption of Acoustical Materials Using a Tube, Two Microphones and a Digital Frequency Analysis System*. Standard. ASTM International.

[238] X Qiu. *Acoustic testing and evaluation of textiles for buildings and office environments. Performance Testing of Textiles: Methods, Technology and Applications: Performance Testing of Textiles: Methods, Technology and Applications, RMIT University, Melbourne, VIC, Australia, pp; 103–128*. 2016.

[239] Tzer Sheng Tie et al. "Sound absorption performance of modified concrete: A review". In: *Journal of Building Engineering* 30 (2020), p. 101219.

[240] Senlin Ling et al. "A comprehensive review of tire-pavement noise: Generation mechanism, measurement methods, and quiet asphalt pavement". In: *Journal of Cleaner Production* 287 (2021), p. 125056.

[241] Fridolin P Mechel and Istvan L Ver. "Sound absorbing materials and sound absorbers". In: *Noise and Vibration Control Engineering, John Wiley & Sons, New York* (1992).